Development of Nanocarbons containing Nitrogen, Oxygen and Tungsten by Solution Plasma Process and their Application as an Electrocatalyst

Md. Zahidul ISLAM

Development of Nanocarbons containing Nitrogen, Oxygen and Tungsten by Solution Plasma Process and their Application as an Electrocatalyst

A Doctoral Dissertation by

Md. Zahidul ISLAM

2021

Department of Chemical Systems Engineering,

Graduate School of Engineering,

Nagoya University, Japan

Table of contents

Abstract

Electrocatalytic activity of Oxygen reduction reaction (ORR) is the most important reaction in the cathode of fuel cell and Li-air battery. The ORR reaction in the fuel cells such as proton exchange membrane fuel cell is significantly slower due to their energy conversion efficiency of fuel cells. Presently, platinum (Pt) is commonly used as a catalyst for ORR but their high cost and long term instability. Presently, in our research group, synthesized the heteroatom-doped carbon materials that show better results in alkaline media compared with Pt, but acid media is lower than that of Pt. Many researchers have also used thermal treatment.

To overcome this problem, this work proposed the tungsten (W) containing nanocarbons compared with the nitrogen (N) and oxygen (O) containing nanocarbon performance of the catalytic activity of ORR and electrical conductivity. The advantage of this work, the solution plasma process (SPP) is successfully synthesis the WC encapsulated nanocarbon from the palm oils, and the N and O containing nanocarbons from the organic solvents. The advantages of palm oil is a low toxicity, chemically inert, inherent biodegradability, and global sustainability compare with organic solvent.The higher synthesis rate is investigated. The enhancement of catalytic activity for ORR in alkali and acid media are evaluated. We investigated that improvement of electrical conductivity and catalytic activity of W, N and O containing nanocarbons without thermal treatment and the commercial Pt/C catalyst using SPP.

In this work, we investigated that palm oil is successfully converted to nanocarbons (W containing) and provided the high electrical conductivity and ORR activity in alkali and acid medium. The organic solvents are synthesized the nanocarbons (N, O and W containing) by SPP with high synthesis rate and catalytic activity site of ORR without thermal treatment and commercial Pt/C catalyst. And the finally, the solid state bio fuel cell fabricated by carbon

nanohorns for biomedical applications.

Chapter 1 shows that overview of this work, especially, the electrocatalytic activity of ORR, present status and issues for nanocarbons and the advantage of the SP process to synthesis the various types of solvent and their problems.

Chapter 2 presents the enhancement of electrical conductivity and Oxidation Reduction Reaction (ORR) activity of tungsten carbide/carbon (WC/C) nanocomposite was successfully synthesized from palm oil by solution plasma process (SPP). The properties of the synthesized WC/C nanocomposite were varied by using a different frequency. The electrical conductivity increased with the frequencies. The highest electrical conductivity was 4.27×10^{-2} S cm^{-1}, which is higher than that of ketjen black (7.37×10^{-3} S cm^{-1}). The WC/C had a surface area of 160 m^2 g^{-1}, a pore volume of 0.53 cm^3 g^{-1}, an average pore diameter of 16.29 nm, a basal plane crystallite size of 18.0 nm, and an average compound granule diameter of less than 100 nm. The cyclic voltammetry measurement was showed that the ORR activity of WC/C was obtained the good performance in alkaline solution for fuel cell application.

Chapter 3 focuses on nanocarbons synthesized by SP from the palm oils. The nanocarbons were covered enhanced electrical conductivity of nanocarbons, which is referred to the nanocarbons-encapsulated WC (tungsten carbides). In this study, we aimed to evaluate the structure and the properties of nanocarbons-encapsulated WC to provide the nanocarbons-encapsulated. The solution plasma was generated by the bipolar pulsed power supply through two tungsten electrodes using 2 μs pulse widths and frequencies (100, 150, and 180 kHz) for 30 min. Conversion percentage of the oil to WC- encapsulated nanocarbon (% yield) was increased with frequency. The obtained X-ray diffraction patterns are showed the crystalline structure. The electrochemical properties indicate that the ORR activity in an acidic medium under saturated O_2 significantly disappears in the case of the nanocarbon-encapsulated WC

synthesised in the high frequency (180 kHz). The synthesized nanocarbons-encapsulated WC might be applied in data storage and energy applications.

Chapter 4 reveals that nanocarbons (N, O and W containing) were successfully synthesized from benzene (BZ), nitro-benzene (BZ-NO_2) and aniline (BZ-NH_2) by Solution Plasma Process (SPP). The synthesized nanocarbons were investigated. The highest synthesis rate of nanocarbon of BZ was 40 mg min^{-1}. The Transmission electron microscopy (TEM) morphology showed that the nanocarbons sizes were 15-25 nm. The cyclic voltammetry (CV) were exhibited in an acidic medium that oxygen reduction reaction (ORR) of nanocarbons. Nanocarbons of BZ-NH_2 have obtained a high special capacity of 15500 mAh/g carbon at the discharge rate of 0.1 mA/cm^2 with the 1.0 mg carbon loading for the lithium (Li)-air battery. An important reaction of ORR in Li-air battery and fuel cells for the applications of next-generation batteries and energy conversion devices.

Chapter 5 shows that this study details the development of a solid-state complementary metal-oxide semi- conductor (CMOS)-compatible bio fuel cell, consisting of various amounts (% wt.) carbon nanohorns (CNHs). It was fabricated on an anode area using one-dimensional (1D) structural CNHs, which express an open-circuit voltage (OCV) of 375 mV, the power density of 8.64 μW/cm^2 and current density 23.05 μA/cm^2 in 30 mM glucose solution. The cell can be manufactured via a CMOS fabrication process, using materials biocompatible with the human body. The CNHs enhanced the fuel cell due to their high electrocatalytic ability. The highest power is 0.42 μW. Power generation is the main challenge for developing bio fuel cells to make the implantable devices that can be used for biomedical applications.

Finally, Chapter 6 summarizes all of the chapters. In this study is to synthesize the nanocarbons from the palm oils and the organic solvent. The W containing nanocarbons and WC encapsulated nanocarbons were successfully synthesized from palm oils by SPP with their

high electrical conductivity, enhanced OOR activity and low synthesis rate compared with N, O and W containing nanocarbons shows the low electrical conductivity, higher electrochemical activity and higher synthesis rate without thermal treatment and the commercial Pt/C catalyst. And the finally, the solid state bio fuel cell is fabricated by carbon nanohorns to make the implantable devices that can be used for biomedical applications.

Chapter 1

General introduction

Chapter 1 – General introduction

1.1 Electrocatalysts for oxygen reduction reaction

The oxygen reduction reaction (ORR) is considered for Li Air Batteries and fuel cells. Figure 1-1 shows the schematic diagram of Li-air Battery. The Li–air battery is shows that the oxidation of lithium in the anode size and the reduction of oxygen in the cathode size and a current flow. Recently, Li-air batteries have been largely used in energy conversion and storage devices for various applications. [1-4] These face the critical challenges that from poor cycle life, low practical energy density, low round-trip efficiency, and high manufacturing costs. To improve the energy storage properties, catalytic activity and less cost, the ORR are demanded. [5-7]

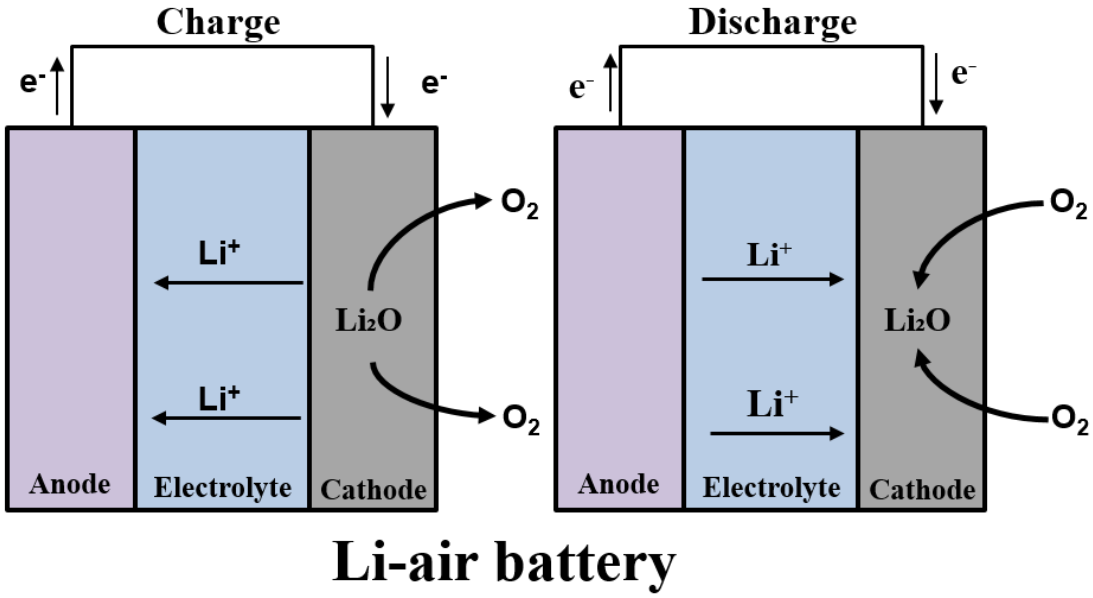

Fig. 1-1 schematic diagram of Li-air Battery.

Figure 1-2 shows the fuel cell connecting with anode, cathode and separator. In the

anode size, When two electrodes and hydrogen gas is injected, hydrogen oxidation reaction occurs. In the cathode size, when oxygen or air is injected, oxygen reduction reaction occurs. ORR is an important reaction in fuel cells. [8, 9] However, ORR in proton exchange membrane fuel cell is significantly slow. [10] This serves as the main factor of limiting energy conversion efficiency of fuel cells. This is why ORR has been a significant research subject of fuel cells.

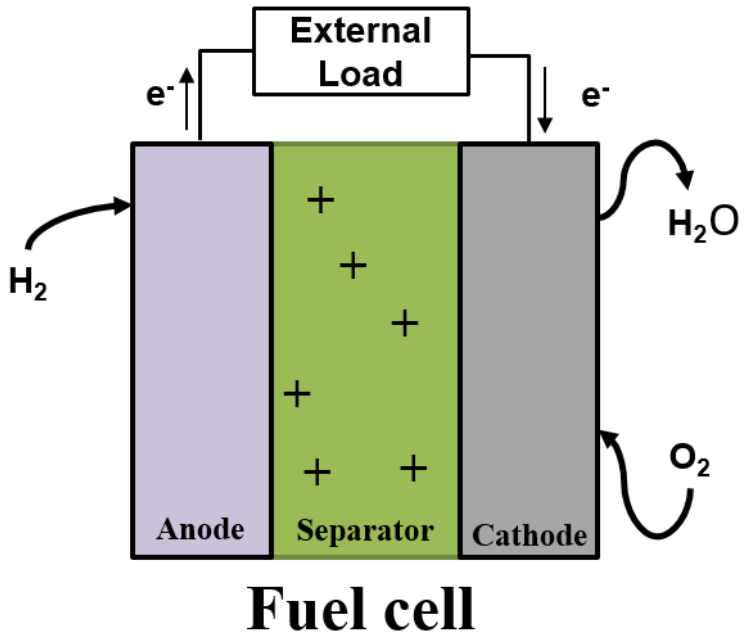

Fig. 1-2 Schematic illustration of fuel cell.

To introduce the alternatives of Pt catalysts, the nanocarbons and heteroatom-doped nanocarbon are attracted. The advantages of the nanocarbons and the heteroatom-doped nanocarbon are the low production cost, excellent chemical properties and the higher electrical conductivity. [11, 12]

1.2 Nanocarbons

1.2.1. *Nanocarbons from palm oils and organic solvents*

The key point of palm oil is constituted by triglyceride (95 - 98%) and minor compounds as mono- and diglycerides (2 - 5%). Triglycerides contain three molecules such as saturated fatty acids, unsaturated fatty acids, and glycerol in the Fig. 1-3. [13] The saturated fatty acids have only a carbon-carbon single bond, and the unsaturated fatty acids contain many carbon-carbon double or triple bonds. Fatty acid composition of palm oil is palmitic acid ($C_{16}H_{32}O_2$, 39%), oleic acid ($C_{18}H_{34}O_2$, 45%), linoleic acid ($C_{18}H_{32}O_2$, 9%), stearic acid ($C_{14}H_{28}O_2$, 5%), and others (2%). [14] Recently, palm oil is used in a fuel cell, bio-based polymers, liquid hydrocarbon fuels and biodiesel. [15-17] The advantages of palm oil consist of low toxicity, chemically inert, inherent biodegradability, and global sustainability. [18] The nanocarbons are successfully produced from the palm oils and organic solvents. [19-25] The nanocarbons such as carbon black, carbon nanotubes, porous and nonporous carbon materials and graphene are showed large specific surface area, high conductivity, electrocatalytic activity, mechanical capacity, ultra-light characteristics, and chemical and thermal resistance. [26-30] In heteroatom (nitrogen, boron, and phosphorus) doped nanocarbon are showed the higher ORR activity. [30-33] Nanocarbons-encapsulated WC is interesting due to core-shell like structure. [34-36]. The core-shell nanostructures were synthesized from polymers and silica. Previously, nanocarbon has been encapsulated from organic solvent. [37-40]

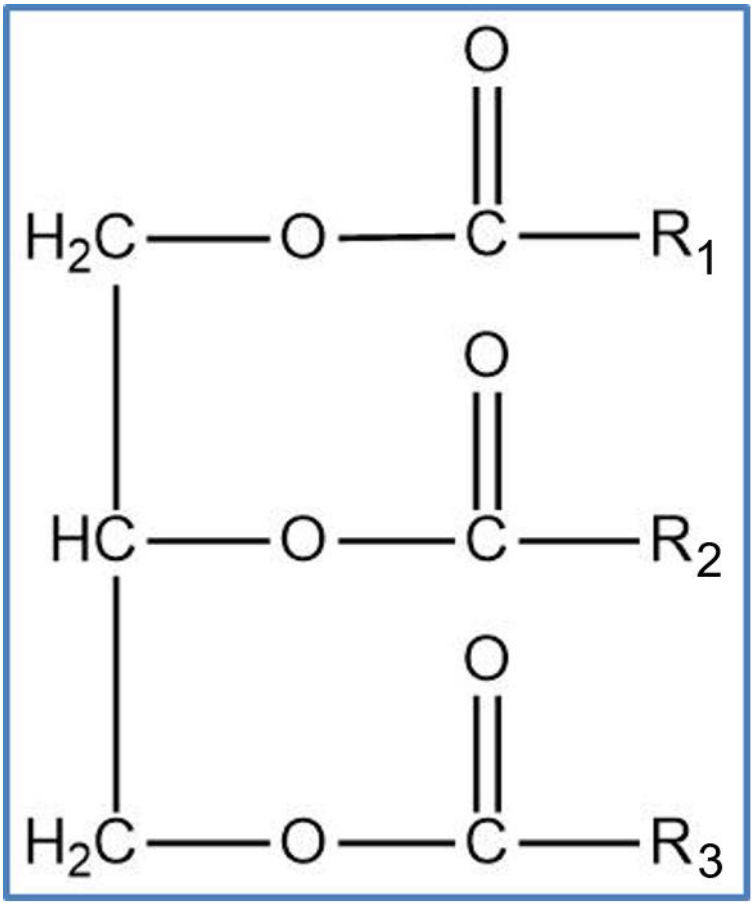

Fig. 1-3 Chemical structure of triglycerides.

Previously, the nanocarbon materials were successfully synthesized by catalytic or nonanalytic chemical vapor deposition, pyrolysis, electric arc discharge, and direct-current (DC) discharge plasma from various organic solvents. [41-43] However, these synthesis technique are complicated due to their high process temperatures, low production yield, and the passing time. [44, 45] And finally nanocarbon such as 1D structural single-walled carbon carbon nanohorns (CNHs) is fabricated on bio (glucose) fuel cells and developed carbon material. [46] It's similar to single-walled carbon nano tubes (SWCNTs). [47] CNHs have possible future applications across a wide range of materials fields. D-Glucose fuel cells are valuable power sources in biomedical areas,

and for human homeostasis. [48, 49]

1.3 Solution plasma process

Solution plasma process (SPP) is a liquid-phase plasma at atmospheric pressures. [50-54] For the synthesis, plasma fields with different frequency were applied the bipolar pulsed power supply between two tungsten electrodes within liquid in the Fig. 1-4. It has attracted a wide range of applications because of its versatility in nanoparticle synthesis, [55] the surface modification of metals, [56] water purification, [57] the polymerization of natural biopolymers, [58] and the functionalization of multi-walled carbon nanotubes (CNTs). [59] In SPP, carbon materials can be synthesized the C–H and C–C single, double and triple bonding as precursors of organic solutions. [60-64]

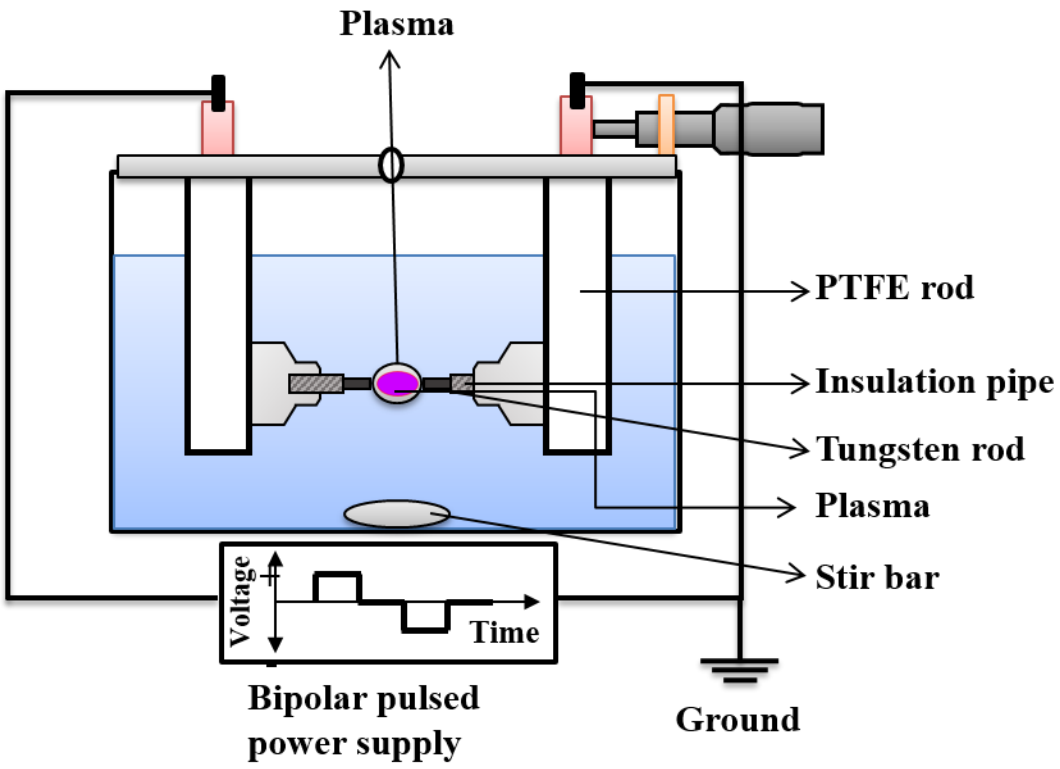

Fig. 1-4 Schematic structure of experimental set-up of solution plasma process.

1.3.1. *Synthesis of nanocarbon from palm oils and organic solvents by SPP*

SPP has many advantages such as simple experimental setup, short time and room temperature and atmospheric pressure. The more advantage of SPP able to synthesis the nanomaterials without any catalyst. SPP is successfully synthesized nanocarbons from the vegetable oils (Palm Oils) in the Fig. 1-5. [65]

Fig. 1-5 Image of solution plasma process (SPP) for the nanocarbon synthesis from palm oil.

Nanocarbons was synthesized from the organic solvent (benzene) by SPP in Fig. 1-6. [66] Recently, solution plasma process has been reported for the synthesis of heteroatom-containing carbons. [67-70] In the case of solution plasma, hetero carbon with catalytic sites may be produced from direct polymerization in the liquid phase.

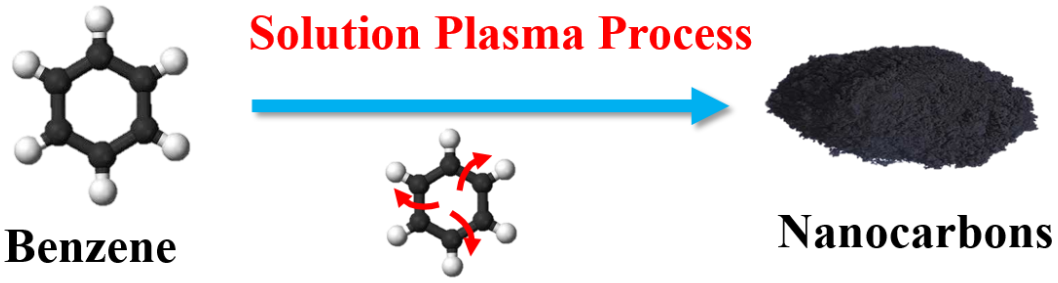

Fig. 1-6 Design of nanocarbons synthesis from benzene by solution plasma process

1.4 Object and outline of the thesis

Purpose of this study is to synthesize the nanocarbons by SPP from the palm oils and the organic solvents. The W containing nanocarbons and WC encapsulated nanocarbons were successfully synthesized from palm oils by SPP with their high electrical conductivity, enhanced ORR activity and low synthesis rate compared with the N, O and W containing nanocarbons of organic solvents (benzene, nitrobenzene and aniline) shows the low electrical conductivity, higher electrochemical activity and higher synthesis rate without thermal treatment and the commercial Pt/C catalyst.

Chapter 1 shows that the electrocatalytic activity of ORR, present status and issues for nanocarbons and the advantage of the SP process to synthesis the various types of solvent and their problems.

Chapter 2 presents the SPP was applied to palm oil to synthesize tungsten carbide/carbon nanocomposite materials with high electrical conductivity. The synthesis WC nanocomposite was analyzed and compared with the commercial carbon Ketjen Black (KB). Most of the conventional processes are time-consuming as compare with SPP.

Chapter 3 focuses on the nanocarbons-encapsulated WC synthesized by SPP from the palm oils. The SPP was generated using A higher 2 μs pulse widths and frequencies (100, 150, and 180 kHz) for 30 min to spattering W in the solution. The electrochemical properties of ORR were showed the nanocarbon entirely encapsulated with WC.

Chapter 4 reveals that N and O containing nanocarbons were successfully synthesized from benzene (BZ), nitro-benzene (BZ-NO_2) and aniline (BZ-NH_2) by SPP. The highest synthesis rate of BZ was 40 mg min-1. The CV was exhibited in an acidic medium that ORR of nanocarbons. N containing Nanocarbons were obtained a high special capacity of 15500 mAh/g carbon at the discharge rate of 0.1 mA/cm2 with the 1.0 mg carbon loading for the Li-air battery compare with palm oils.

Chapter 5 shows that this study details the development of a solid-state complementary metal-oxide semi- conductor (CMOS)-compatible bio fuel cell, consisting of various amounts (% wt.) carbon nanohorns (CNHs). It was fabricated on an anode area using one-dimensional (1D) structural CNHs, which express an open-circuit voltage (OCV) of 375 mV, the power density of 8.64 $\mu W/cm^2$ and current density 23.05 $\mu A/cm^2$ in 30 mM glucose solution. The fuel cell can be manufactured via a CMOS fabrication process, using materials biocompatible with the human body. The CNHs enhanced the fuel cell due to their high electrocatalytic ability. The highest power is 0.42 μW. Power generation is the main challenge for developing bio fuel cells to make the implantable devices that can be used for biomedical applications.

Finally, Chapter 6 summarizes all of the chapters.

References

1) S. W. Lee, N. Yabuuchi, B. M. Gallant, S. Chen, B.-S. Kim, P. T. Hammond and Y. Shao-Horn, Nat. Nanotechnol., 5, 531 (2010).
2) A. Chen and P. Holt-Hindle, Chem. Rev., 110, 3767 (2010).
3) X. Ma, H. Meng, M. Cai and P. Shen, J. Am. Chem. Soc., 134, 1954 (2012).
4) Y. Zhao, L. Yang, S. Chen, X. Wang, Y. Ma, Q. Wu, Y. Jiang, W. Qian and Z. Hu, J. Am. Chem. Soc., 135, 1201 (2013).
5) F. R. Brushett, M. S. Thorum, N. S. Lioutas, M. S. Naughton, C. Tornow, H. R. M. Jhong, A. A. Gewirth, and P. J. A. Kenis, J. Am. Chem. Soc., 132, 12185 (2010).
6) N. A. Anastasijevic, V. Vesovic, and R. R. Adzic, J. Electroanal. Chem., 229, 305 (1987).
7) Y. Feng, A. Gago, L. Timperman, and N. Alonso-Vante, Electrochim. Acta, 56, 1009 (2011).
8) B. Wang, J. Power Sources, 152, 1 (2005).
9) M. K. Debe, Nature, 486, 43 (2012).

10) Y. Liu, A. Ishihara, S. Mitsushima, N. Kamiya, and K. Ota, J. Electrochem. Soc., 154, B664 (2007).

11) J. Kim, T. Oh, Y. Shin, J. Bonnett, and K. Weil, Int. J. Hydrogen Energy, 36, 4557 (2011).

12) J. Snyder, T. Fujita, M.W. Chen, and J. Eelebancher, Nat. Mater., 9, 904 (2010).

13) Y. Nie, L. Li, and Z. Wei, Chem. Soc. Rev., 44, 2168 (2015) G. Wang, G. Sun, Q. Wang, S. Wang, H. Sun, and Q. Xin, Int. J. Hydrog. Energy, 35, 11245-11253 (2010).

14) A. B. Suriani, A. Aziz, S. F. Nik, R. M. Nor, and M. Rusop, Mater. Lett., *63*, 2704-2706 (2009).

15) R. Kumar, R. K. Singh, and D. P. Singh, Renew. Sustain. Energy Rev., 58, 976-1006 (2016).

16) J. K. Sudesh, K. Bhubalan, J. A. Chuah, Y. K. Kek, H. Kamilah, N. Sridewi, and Y. F. Lee, Appl. Microbiol. Biotechnol., *89*, 1373-1386 (2011).

17) Y. Xia, and R. C. Larock, Green Chem., 12, 1893-1909 (2010).

18) G. Lligadas, J. C. Ronda, M. Galia, and V. Cadiz, Mater. Today, 16, 337-343 (2013).

19) V. I. Zaikovskii, K. S. Nagabhushana, V. V. Kriventsov, K. N. Loponov, S. V. Cherepanova, R. I. Kvon, D. I. Kochubey, and E. R. Savinova, J. Phys. Chem. B, 110, 6881(2006).

20) K. Jukk, N. Alexeyeva, P. Ritslaid, J. Kozlova, V. Sammelselg, and K. Tammeveski, Electrocatalysis, 4, 42 (2013).

21) R. Zhou and S. Qiao, Chem. Mater., 26, 5868 (2014).

22) J. Qiao, R. Lin, B. Li, J. Ma, and J. Liu, Electrochim. Acta, 55, 8490 (2010).

23) M. H. Shao and R. R. Adzic, Langmuir, 22, 10409 (2006).

24) Y. G. Suo and L. Zhuang, Angew. Chem., Int. Ed., 46, 2862 (2007).

25) C. W. B. Bezerra, L. Zhang, K. Lee, H. Liu, A. L. B. Marques, E. P. Marques, H. Wang, and J. Zhang, Electrochim. Acta, 53, 4937 (2008).

26) Y. Hu, W. Xing and Q. Li, Angew. Chem., Int. Ed., 53, 3675 (2014).

27) D. W. Kim, O. L. Li, and N. Saito, Phys. Chem. Chem. Phys., 16, 14905 (2014).

28) R.J. Toh, Z. Sofer, and M. Pumera, Chem. Phys. Chem., 16, 3527 (2015).

29) M. R. Gao, J. Jiang, and S. H. Yu, Small, 8, 13 (2012).

30) B. Cao, J. C. Neuefeind, R. R. Adzic, and Peter G. Khalifah, Inorg. Chem., 54, 2128 (2015).

31) D. S. Yu, E. Nagelli, F. Du, and L. M. Dai, J. Phys. Chem. Lett., 1, 2165 (2010).

32) S. Doi, A. Ishihara, S. Mitsushima, N. Kamiya, and K. I. Ota, J. Electrochem. Soc., 154, B362 (2007).

33) Y. J. Wang, D. P. Wilkinson, and J. J. Zhang, Chem. Rev. 111, 7625 (2011).

34) S. Dou, A. Shen, L. Tao, and S. Wang, Chem. Commun., 50, 10672 (2014).

35) J. Liu, X. Sun, P. Song, Y. Zhang, W. Xing, and W. Xu, Adv. Mater., 25, 6879 (2013).

36) J. Liang, X. Du, C. Gibson, X. W. Du, and S. Z. Qiao, Adv. Mater., 25, 6226 (2013).

37) S. Wang, E. Iyyamperumal, A. Roy, Y. Xue, D. Yu, and L. Dai, Angew. Chem., Int. Ed., 50, 11756 (2011).

38) C. Xiong, Z. Wei, B. Hu, S. Chen, L. Li, L. Guo, W. Ding, X. Liu, and W. Ji, X. Wang, J. Power Sources, 215, 216 (2012).

39) L. Yang, S. Jiang, Y. Zhao, L. Zhu, S. Chen, X.Wang, Q.Wu, J. Ma, Y. Ma, and Z. Hu, Angew. Chem. Int. Ed., 50, 7132 (2011).

40) J. Zhang, Z. Zhao, Z. Xia, and L. Dai1, Nat. Nanotechnol., 10, 444 (2015).

41) Z. Ma, S. Dou, A. Shen, L. Tao, L. Dai, and S. Wang, Angew. Chem. Int. Ed., 53, 1 (2014).

42) X. Sun, Y. Zhang, P. Song, J. Pan, L. Zhuang, W. Xu, and W. Xing, ACS Catal., 3, 1726 (2013).

43) Y. Zhan, J. Huang, Z. Lin, X. Yu, D. Zeng, X. Zhang, F. Xie, W. Zhang, J. Chen, and H. Meng, Carbon, 95, 930 (2015).

44) Z. Jin, H. Nie, Z. Yang, J. Zhang, Z. Liu, X. Xu, and S. Huang, Nanoscale, 4, 6455 (2012).

45) G. Liu, X. Li, P. Ganesan, and B. N. Popov, Electrochim. Acta, 55, 2853 (2010).

46) S. Iijima, M. Yudasaka, R. Yamada, S. Bandow, K. Suenaga, F. Kokai and K. Takahashi, Chem. Phys. Lett. **309**, 165–170 (1999).

47) M. Z. Islam, S. Arata, K. Hayashi, A. Kobayashi, and K. Niitsu, Nanosci. Nanotechnol. Lett.,12, 101-106 (2020).

48) Jr. L.B. W., C. H. Shaw, and J. F. Castner, Enzyme Microb. Technol. 4 (3): P 6 (1982).

49) A. Kobayashi, K. Ikeda, Y. Ogawa, H. Kai, M. Nishizawa, K. Nakazato, and K. Niitsu, IEEE Trans. Biomed. Circuits Syst. **11**, 1313 (2017).

50) O. Takai, Pure Appl. Chem., 80, 2003 (2008)

51) P. Q. Phan, S. Chae, P. Pornaroontham, Y. Muta, K. Kim, X. Wang, N. and Saito, RSC Adv., 10, 36627–36635 (2020).

52) N. Saito, J. Hieda, O. Takai, Thin Solid Films, 518, 912-917 (2009).

53) A. Watthanaphanit, and N. Saito, Jpn. J. Appl. Phys., 57, 0102A3 (2018).

54) N. Saito, M. A. Bratescu, K. Hashimi, Jpn. J. Appl. Phys., 57, 0102A4 (2018).

55) G. Mehta, A. K. Mohanty, M. Misra, and L. T. Drzal, Green Chem., 6, 254-258 (2004).

56) M. Z. Islam, A. Watthanaphanit, S. Chae, and N. Saito, Nanosci. Nanotechnol. Lett., accepted (2020).

57) N. Taufiqurrahmi, and S. Bhatia, Energy Environ. Sci., 4, 1087-1112 (2011).

58) N. Saito, N., T. Ueno, M. A. Bratescu, and J. Hieda, Novel Structured Metallic and Inorganic Materials, 343-355 (2019).

59) A. Watthanaphanit, G. Panomsuwan, and N. Saito, RSC Adv., 4, 1622–1629 (2014).

60) S. Chae, K. Hashimi, M. A. Bratescu, and N. Saito, Nanosci. Nanotechnol. Lett., 10, 784-789 (2018).

61) S. Chae, G. Panomsuwan, M. A. Bratescu, K. Teshima, and N. Saito, ACS Appl. Nano Mater., 2, 1350−1355 (2019).

62) T. Sudare, T. Ueno, A. Watthanaphanit, and N. Saito, J. Phys. Chem. A., 119, 11668−11673 (2015).

63) S. Nemoto, T. Ueno, A. Watthanaphanit, J. Hieda, M. A. Bratescu, and N. Saito, Jpn. J. Appl. Phys., 56, 096202 (2017).

64) T. Shirafuji, J. Ueda, A. Nakamura, S. P. Cho, N. Saito, and O. Takai, Jpn. J. Appl. Phys., 52, 126202 (2013).

65) P. Meeprasertsagool, A. Watthanaphanit, T. Ueno, N. Saito, and P. Reubroycharoen, Energy Procedia 138, 1153-1158 (2017).

66) A. Watthanaphanit and N. Saito, Polym. Degrad. Stab., 98, 1072 (2013).

67) T. Shirafuji, Y. Noguchi, T. Yamamoto, J. Hieda, N. Saito, O. Takai, A. Tsuchimoto, K. Nojima, and Y. Okabe, Jpn. J. Appl. Phys., 52, 125101 (2013).

68) G. Panomsuwan, S. Chiba, Y. Kaneko, N. Saito, and T. Ishizaki, J. Mater. Chem. A, 2, 18677 (2014).

69) O. L. Li, J. Kang, K. Urashima, and N. Saito, Int. J. Environ. Sci. Technol., 7, 31 (2013).

70) D. W. Kim, O. L. Li, and N. Saito, Phys. Chem. Chem. Phys., 17, 407 (2015).

Chapter 2

Synthesis of tungsten carbide/carbon nanocomposite from palm oil by solution plasma process and their oxygen reduction reaction

Chapter 2 - Synthesis of tungsten carbide/carbon nanocomposite from palm oil by solution plasma process and their oxygen reduction reaction

2.1. Introduction

Recently, palm oil (a type of vegetable oil) starts to be a more attractive material with economic benefits because it is made from renewable resources and can be a component in many manufactured products. Palm oil is produced in South-east Asia and Africa, mainly in Malaysia and Indonesia from where is considered the cheapest and available biological feedstock in large quantities. The advantages of palm oil consist of low toxicity, chemically inert, inherent biodegradability, and global sustainability. [1-3] The palm oil is successfully used in a fuel cell, bio-based polymers, liquid hydrocarbon fuels and biodiesel. [4-6]

Recently the properties of carbon materials vary in a wide range from a sp^2 structure in carbon black, nanocarbon, carbon nanotubes (CNT), graphene, porous and nonporous carbon materials, a mixed sp^2 - sp^3 structure as in diamond-like materials, and sp^3 structure in the diamond. The nanocarbon materials have unique properties, such as a large specific surface area, high conductivity, electrocatalytic activity, mechanical capacity, ultra-light characteristics, and chemical and thermal resistance. [7-14] However, one of the most significant nanocarbon properties is electrical conductivity. It also has been performed in the nanocarbon composites, carbon nanotube, nanocarbon black, and graphene sheets. [15-26]

Previously, the nanocarbon materials were synthesized by catalytic or nonanalytic chemical vapour deposition, pyrolysis, electric arc discharge, and direct-current (DC) discharge plasma from various organic solvents. [27-30] However, these synthesis methods are complicated due to

their high process temperatures, low production yield, and prolonged treatment time. [31] Recently a non-equilibrium liquid-phase plasma called Solution Plasma Process (SPP) was used to synthesize carbon materials at room temperature, and atmospheric pressure. [32-35] SPP is one of the saving energy processes where nanocarbon can be rapidly synthesized. In our laboratory, we conducted various experiments to produce carbon materials from organic solvents by SPP. [36]

In this research, for the first time, SPP was applied to palm oil to synthesize nanocarbon materials with a high electrical conductivity that might be useful for the production of metals like-plastics and composites. The results show that the most significant issue of palm oil processed by SPP consists of high efficiency for nanocarbon production. The crystallinity, structure, surface area, morphology, and electrochemical activity of nanocarbon were analyzed and compared with the commercial carbon Ketjen Black (KB). Most of the conventional processes are time-consuming as compare with SPP. [37] Besides, the interesting part of nanocarbon has a potential application on ORR for fuel cells and related applications.

2.2. Experimental procedure

2.2.1 *Materials*

Palm oil (Kobe Busan Co., Ltd. Japan) (100% vegetable cooking oil) was selected as a material for the nanocarbon synthesis. Ketjen Black (KB, Lion Specialty Chemicals Co., Ltd. Japan), Polyvinylidene Fluoride (PVDF, Sigma-Aldrich, Japan), N-Methyl-2-pyrrolidone (NMP, Kanto Chemical Co., INC, Japan), Acetone (Kanto Chemical Co., INC, Japan) and Ethanol (Kanto Chemical Co., INC, Japan) were purchased.

2.2.2 *Experimental setup and production procedure*

Transmission The experimental setup of SPP is shown in Fig. 2-1. The plasma was generated using a bipolar pulsed power supply (MPS-R06K01C-WP1-6CH, Kurita Co. Ltd., Japan) between two tungsten (W) electrodes (wire type, purity 99.9%, The Nilaco Corporation, Japan) with a 1 mm diameter, covered with an insulating ceramic tube. The electrode gap was 0.5 mm in the beginning. The applied high voltage had different pulse widths (1 and 2 μs) and repetition frequencies (15, 25, 40, and 50 kHz). The processing time was 40 min. The current and voltage waveforms were observed using an oscilloscope (DLM 2022, Yokogawa Meters & Instruments Corporation, Japan) in the range of 0 – 5 A and 0.6 - 1.0 kV, respectively.

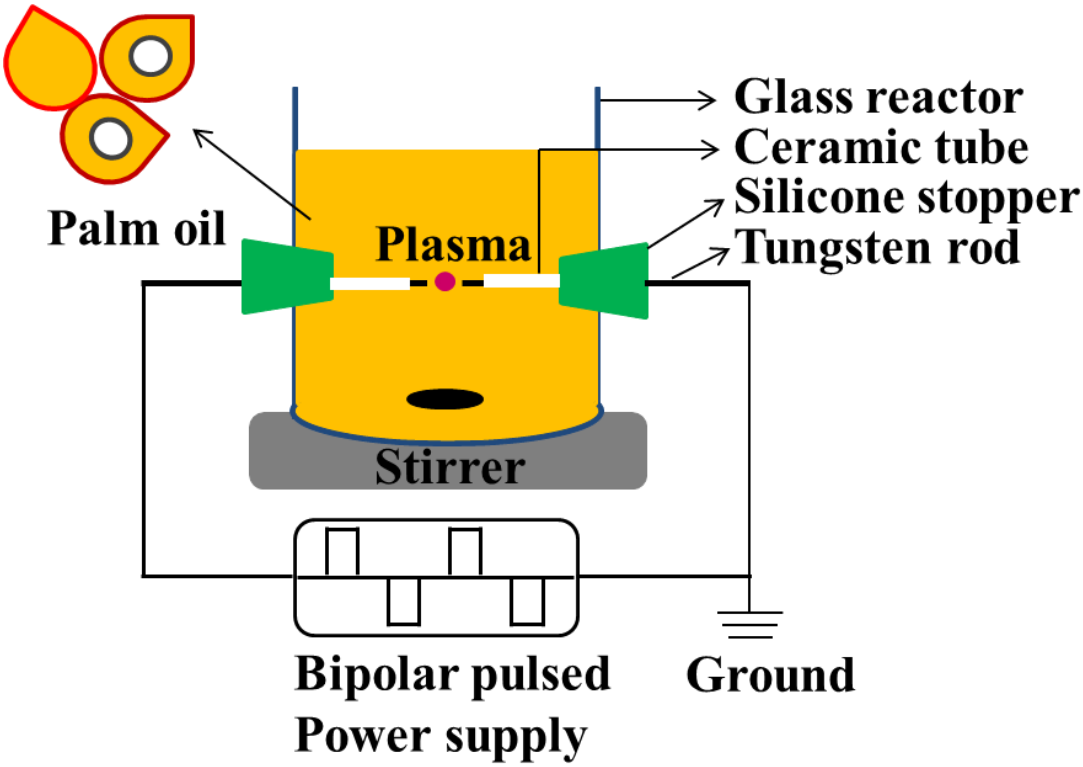

Fig. 2-1 Schematic illustration of solution plasma process (SPP) for the nanocarbon materials synthesis from palm oil.

During SPP, the electrodes were adjusted several times, especially at high frequencies of SPP operation (i.e., 40 and 50 kHz) to keep a constant gap distance between the electrodes. Due to

erosion, the electrode gap distance increases. This adjustment also has a role in maintaining stable plasma during the process. If the electrode gap distance increases from 0.5 mm to 1 mm or more, the discharge stops. After the nanocarbon materials synthesis, the liquid and solid phases were separated by centrifugation. The solid phase was washed three times with acetone until the oils have been entirely removed using centrifugation at 12000 rpm for 30 min and then dried at 90° C for six hours in an oven (DX301, Yamato Co. Ltd., Japan). The weight of nanocarbon was measured using a balance (EK2000i, AS-ONE Co. Ltd., Japan).

2.2.3 *Characterization*

The properties of the structure were investigated by X-ray diffraction (XRD, Rigaku Smart lab, Rigaku Corporation, Japan) with a Cu Kα X-ray radiation source at λ = 0.154 nm in the 2Θ range from 3.0 to 90.0 degrees and a scan speed of 3.0 degrees. Raman spectroscopy (NRS-100, JASCO Corporation, Japan) used the wavelength of 532.5 nm and 1 mW power to determine the type of nanocarbon material. The X-ray Photoelectron Spectroscopy (XPS, PHI 5000 Versa Probe II; Ulvac-Phi physical Electronics INC, Japan) measured the elemental composition using the Mg Kα X-ray source with the energy of the photon of 1253.6 eV. The morphology, shape, and size of nanocarbon were observed by Scanning Electron Microscopy (SEM, JSM-7100F, JEOL Ltd., Japan) with an accelerating voltage of 15 kV and a working distance of 10 mm. Transmission electron microscopy (TEM, JEM-2500SE, JEOL Ltd., Japan) with an electron gun at 200 kV was used to analyze the size and crystallinity of the synthesized nanocarbon. The Brunauer-Emmett-Teller (BET, BELSORP-mini-II, BEL JAPAN, INC, Japan) device measured the surface area, pore volume, and average pore diameter from the nitrogen adsorption-desorption isotherms at 77 K. The electrical resistivity and electrical conductivity were investigated by a four-point probe method (Laresta-GP, MCP-T610, Mitsubishi Chemical Analytech Co., Ltd., Japan). A concentration of 60 *wt*% of nanocarbon was mixed with 40 *wt* % polymer binder (PVDF) and then sonicated in NMP for 30 min. The emulsion was dropped on

a glass substrate and then dried in an electric oven at 120 ºC for 20 min to form a uniform film.

Electrochemical measurements were carried out on a computer-controlled ALS-CH model 704 ES electrochemical analyzer (CH instrument Inc.). The ink made by catalyst (5.0 mg), ultrapure water (480 mL), ethanol (480 mL), and Nafion® aqueous solutions (40 mL) were ultra-sonicated was obtained. The Ag/AgCl solution was applied as the counter and reference electrodes by cyclic voltammetry (CV) at 0.1 M KOH solution. In additions, O_2 gas was saturated in 0.1 M KOH solutions at 20 min.

2.3. Results and discussion

2.3.1. *Structural properties and compositions*

The primary fatty acids of palm oil are palmitic ($C_{16}H_{32}O_2$) and oleic acid ($C_{18}H_{34}O_2$). To obtain carbon from palm oil in SPP the decomposition of molecules is necessary. Plasma breakdown occurs by a combination of two processes. One process is related to the solution conductivity which leads to liquid heating, vaporization, and breakdown in bubbles. The second process is determined by the dielectric strength of the liquid which conducts to electron acceleration in the electric field, primary ionization followed by electron avalanche and breakdown. In any case after plasma breakdown, the molecules are dissociated and ionized due to the plasma synthesis reaction occur in the liquid phase. SPP has two interfaces plasma/gas and gas/liquid. In the plasma gas phase, the main processes are excitation, ionization, dissociation of molecules generating excited species, ions, radicals, atoms, and photons. [32, 33] These species subsequently act as the initiator and preserving source for the chemical reactions.

The XRD patterns showed two peaks at 24.5° and 43.5°, corresponding to the 0 0 2 and 1 0 1 graphite planes (JCPDS 75-1621). Nanocarbon synthesized at different frequencies exhibited a relatively broad peak for the 0 0 2 planes, except for KB, as shown in Fig. 2-2. These results indicated amorphous carbon. When the energy increased, the 0 0 2 peaks also sharply increased.

[17] The 1 0 1 peak was observed among graphite and amorphous position, indicating a turbostratic structure. In addition, the WC (JCPDS #25-1047) peaks corresponded to the 1 1 1, 2 0 0, 2 2 0, 3 1 1, and 2 2 2 planes. [35, 36]

These results indicate that when the frequency is higher, the WC peaks gradually increased due to a higher sputtering of the tungsten electrode. Due to the big difference between the shapes of the XRD diffractions of WC 200 and carbon 100/101, these peaks can be easily distinguished. The frequency influences the sputtering. The high current determines a high number density of ions, while high voltage implies a high acceleration of the ions in plasma. [37]

The surface elemental composition was identified by XPS as shown in Fig. 2-3 (a). The percentages of nanocarbon (88.0, 89.5, 90.7, and 91.6 atom %), oxygen (11.8, 10.1, 9.2, and 7.8 atom %), and tungsten (0.2, 0.4, 0.5, and 0.6 atom %) were identified for different amount of frequencies and are plotted in Fig. 2-3 (b).

The composition ratio increased with frequency. In the low frequency, the hydrocarbon cracking and tungsten sputtering rate is low compared with the high input energy case. XPS of the nanocarbon composite showed significant peaks corresponding to C 1s, O 1s, and W 1s. When the frequency increased, then the cracking rate, carbon, and tungsten composition also increased. During SPP synthesis, from fatty acids, CO, CO_2, water, and hydrocarbons are also produced. The percentage of oxygen decreased due to these gases eliminated during palm oil decomposition. [34-38]

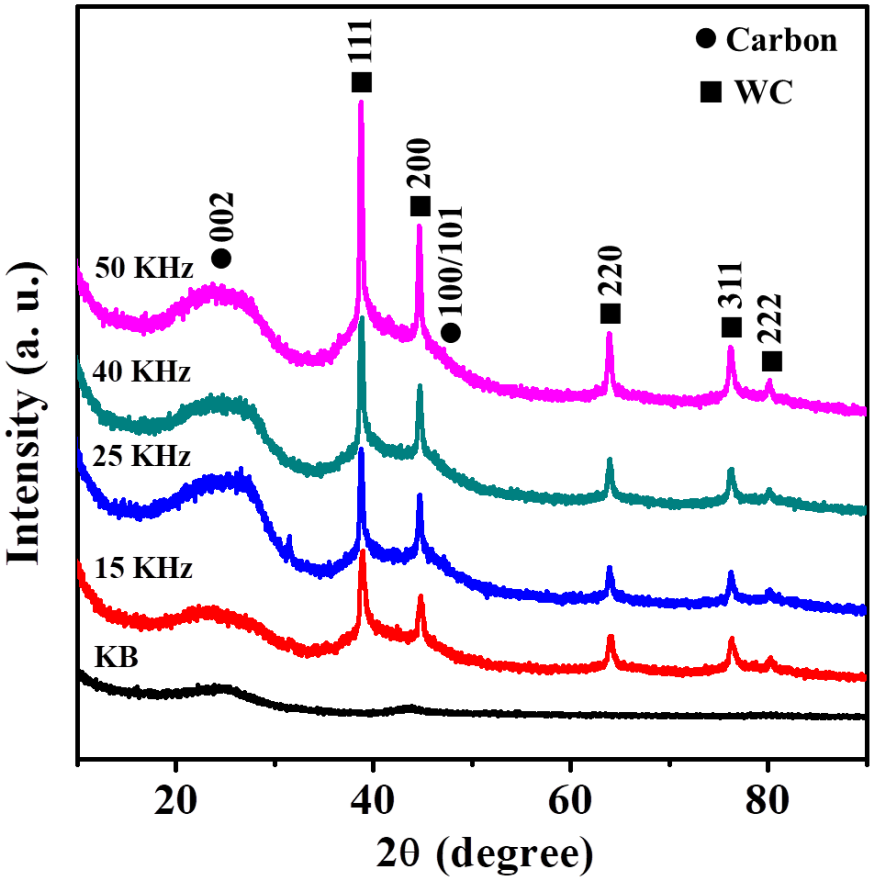

Fig. 2-2 XRD patterns of nanocarbon powders from palm oil of various amount frequencies 15, 25, 40 and 50 kHz in 2μs at 40 min discharge with commercial carbon KB respectively.

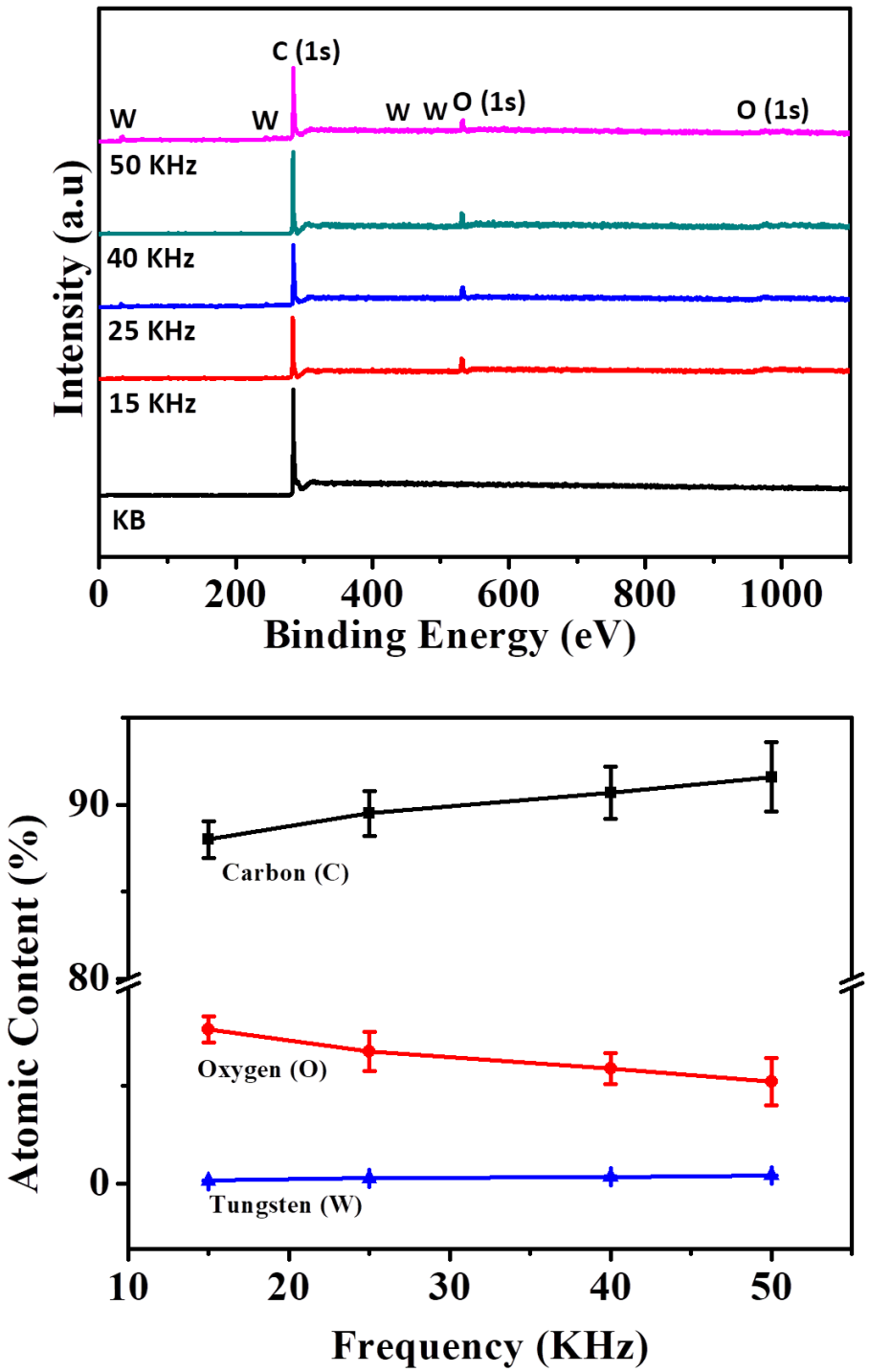

Fig. 2-3 a) XPS spectra for a pulse width of 2 μs with frequencies of 15, 25, 40 and 50 KHz. Chemical structure of triglycerides and b) Summary of XPS elemental compositions (% atom) of nanocarbon for 2 μs were obtained from palm oil.

2.3.2. *Morphology*

The SEM images display nanocarbon morphologies obtained at low and high frequency; as shown in Fig. 2-4 (a, b, c), the nanocarbon is spherical. The size distribution of nanocarbons was determined a broad, ranging from 30 to 90 nm for both low and high frequency. When the frequency increased, the nanocarbon size decreased. At high plasma energy, spherical nanocarbon similar to Ketjen Black (KB) was observed, as shown in Fig. 2-4 (a).

The morphology of nanocarbon was observed using TEM as shown in Fig. 2-4 (a′, b′, and c′), high-resolution TEM (HR- TEM) as shown in Fig. 2-4 (a″ b″, and c″), and selected area diffraction (SEAD), inset in the HR-TEM images. The TEM images show the observed nanocarbon were spherical shape type morphology, while the HR-TEM and SEAD patterns show that the obtained nanocarbon is an amorphous structure at all frequencies.

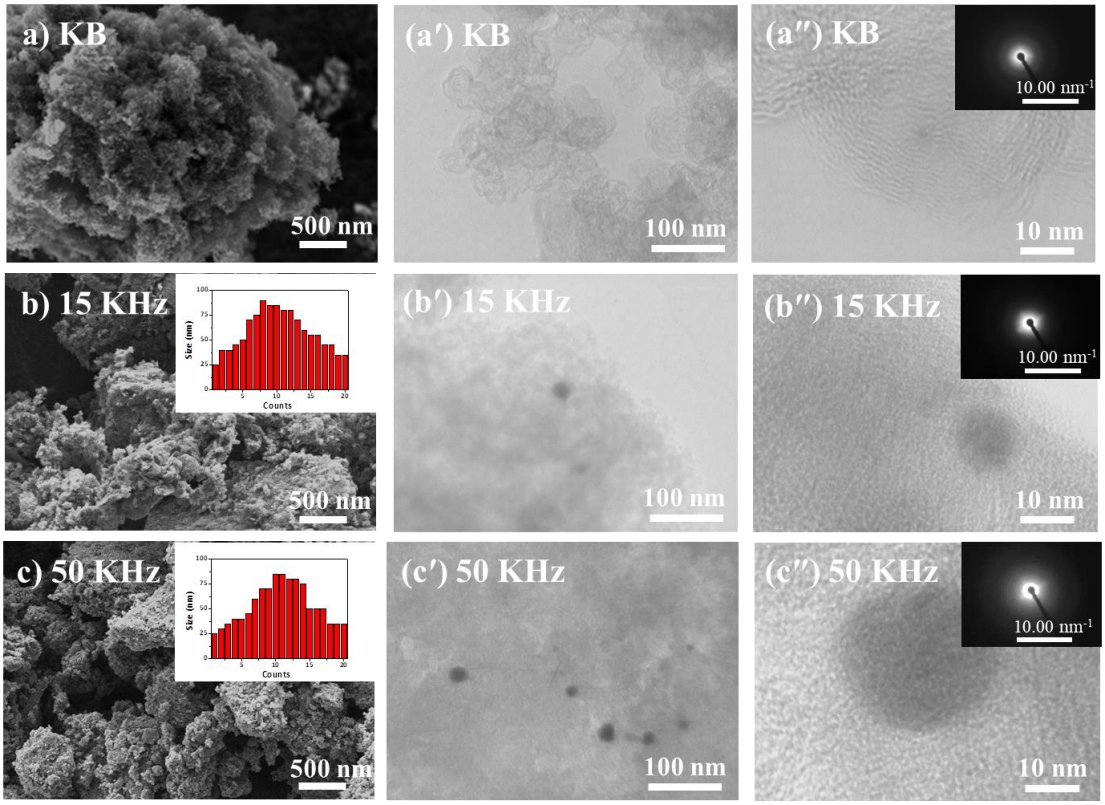

Fig. 2-4 SEM, TEM and HR-TEM images of nanocarbon correspond with SEAD pattern (insert) from palm oil, a, b and c) SEM image; a′, b′and c′) TEM image and a″, b″ and c″) HR-TEM at 2 μs pulse width.

2.3.3. *Electrical resistivity test*

The four-point probe method was applied to the nanocarbon to identify the resistance (Ω), surface resistance (Ω/cm^2), resistivity (Ω.cm), and electrical conductivity (s/cm) as shown in Table 2-1.

Table 2-1 The resistance (Ω), surface resistance (Ω/cm^2), resistivity (Ω.cm), and electrical conductivity (s/cm) tested with the four-point probe under different conditions.

Conditions	Film thickness (μm)	Resistance (Ω)	Surface restance (Ω/cm^2)	Electrical conductivity (s/cm)	Resistivity (Ω.cm)
15 kHz	134	2.35×10^3	1.06×10^4	2.29×10^{-2}	43.6
25 kHz	121	1.06×10^3	4.79×10^3	2.11×10^{-2}	40.7
40 kHz	125	7.18×10^2	3.25×10^3	2.93×10^{-2}	34.2
50 kHz	140	1.32×10^3	6.00×10^3	4.27×10^{-2}	23.4
KB	139	5.16×10^3	2.34×10^4	7.37×10^{-3}	135.7

The resistivity (Ω.cm) of nanocarbon is lower than that of KB, because of its hydrogen (H) and tungsten carbide (WC) content. [30] Thus, we observed that when the resistivity (Ω.cm) of the nanocarbon decreased, its conductivity increased, and the 50 kHz frequency gave the highest conductivity compared with other frequency as shown in Fig. 2-5. The high conductivity at high frequency is due to the high amount of WC and the less amount of H in the material.

Finally, we concluded that palm oils could be used to synthesize nanocarbon by SPP using different amount of frequencies. When the frequency increased, the plasma temperature also increased, so that more carbon-carbon bonds were cracked, and the cracking rate also increased. Thus, the mass of nanocarbon composite increased when the frequency increased, as shown by all the data.

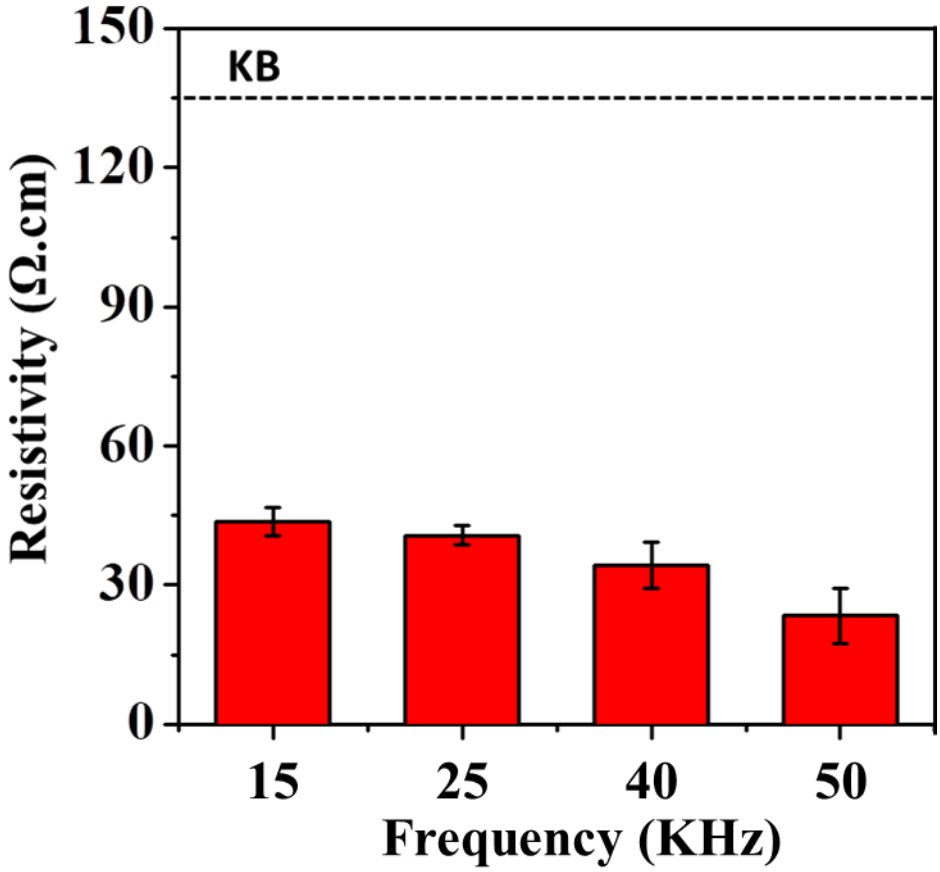

Fig. 2-5. Electrical resistivity (Ω.cm) vs. frequency compared with KB.

2.3.4. *Raman and surface area*

Raman spectroscopy showed D and G bands at 1350 and 1580 cm^{-1}. Structural disorder and a sp^2 graphite sheet-like structure were inferred from the D and G bands, respectively. The I_D/I_G ratios for the nanocarbon formed with 15, 25, 40, and 50 kHz were, respectively, 0.98, 0.99, 1.00 and 1.06, calculated from the peak heights as shown in Fig. 2-6, as compared with that of KB (1.23). The I_D/I_G ratio increased with the pulse frequency. These results showed that the sp^2 content of nanocarbon increased, together with its sheet-like structure and bond disorder. The 2D peak at 2600–2750 cm^{-1} confirms that nanocarbon has relatively high basal plane

crystallinity. The I_G/I_D ratio is inversely proportional to the crystallite size L_a as follows.

L_a (nm) = $(2.4 \times 10^{-10}) \lambda^4 (I_G/I_D)$, [38]

where λ is the Raman excitation wavelength at 532 nm.

The crystallite sizes L_a (nm) decreased from 19.6 to 18.1 nm as the frequency increased. These results indicate that nanocarbon production increases with frequency and nanocarbon composite materials are amorphous with a low degree of crystallinity. Therefore, D′-band was not detected in the Raman spectrum. [39] The deconvolution of the Raman spectra is shown in Fig. 2-7.

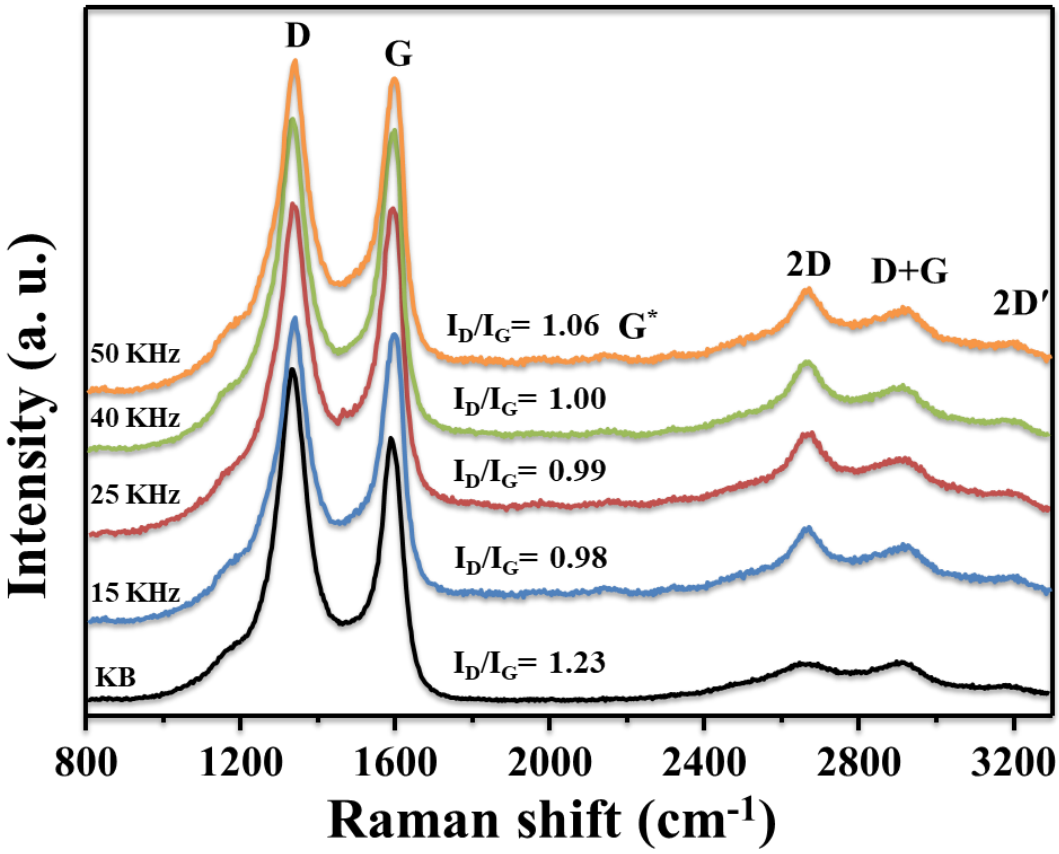

Fig. 2-6 Raman spectra of nanocarbon from frequencies 15, 25, 40 and 50 KHz with commercial carbon KB, respectively.

The surface area, pore volume, and average pore diameters were determined by BET measurements using N_2 adsorption-desorption isotherms as shown in Table 2-2. As the frequency increases, the surface area, pore volume, and average pore diameter of nanocarbon

change from 101 to 160 $m^2 g^{-1}$, 0.23 to 0.53 $cm^3 g^{-1}$, and 20.08 to16.29 nm, respectively. This result indicates that when the frequency increases, the crystallite size and average pore diameter decreases, and the surface area increase. [40] High plasma energy determines more decomposition and less hydrogen in the nanocarbon composition resulting in the increasing of the crystallite size.

Table 2-2 Carbon particle analysis from palm oil by using Brunauer, Emmett and Teller (BET) theory measurement.

Conditions	Average pore diameter (nm)	Pore volume (cm^3/g)	Surface area (m^2/g)
50 kHz, 2μs, 40 min	20.08	0.23	101
15 kHz, 2μs, 40 min	16.29	0.53	160
Ketjen Black (KB)	8.06	2.25	1120

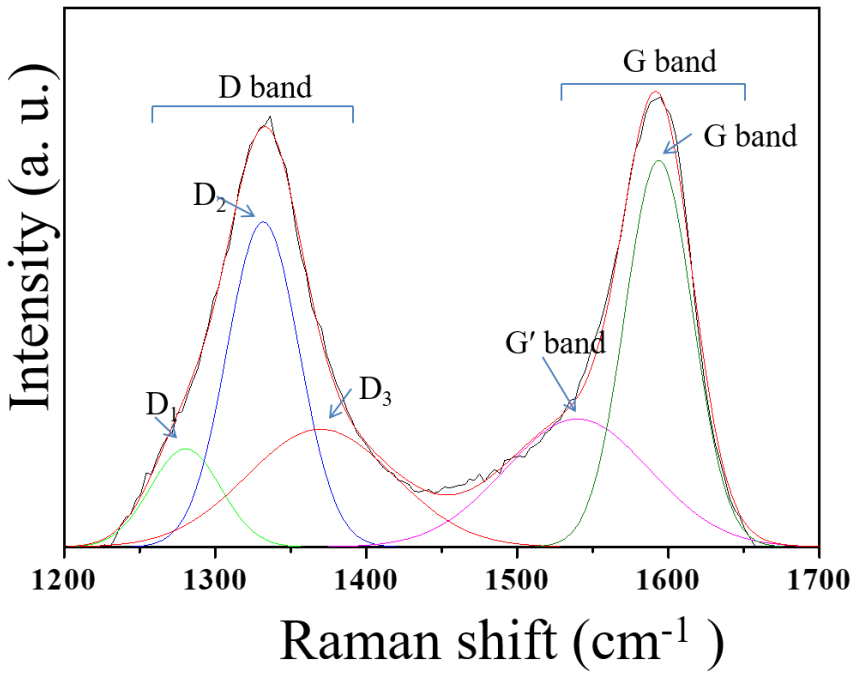

Fig. 2-7 Deconvolution of the Raman spectra of the nanocarbon composite for 50 KHz.

2.3.5. *Electrocatalytic activity of ORR*

The electrocatalytic activity of ORR of 15 and 50 kHz were evaluated by cyclic voltammetry (CV) in 0.1 M KOH solution. The CV curves in 0.1 M KOH solutions with O_2 saturated were 30 cycles in the potential range from -1.0 to 0.3 V at a scan rate of 50 mV s^{-1} at Fig. 2-8. The ORR peak slightly improved. The onset potential is to quit a few current densities for the ORR. Nanocarbon with high specific surface area is promoting ORR activity. However, in our study, the ORR activities of nanocarbon perform once quit lower than electrical conductivity.

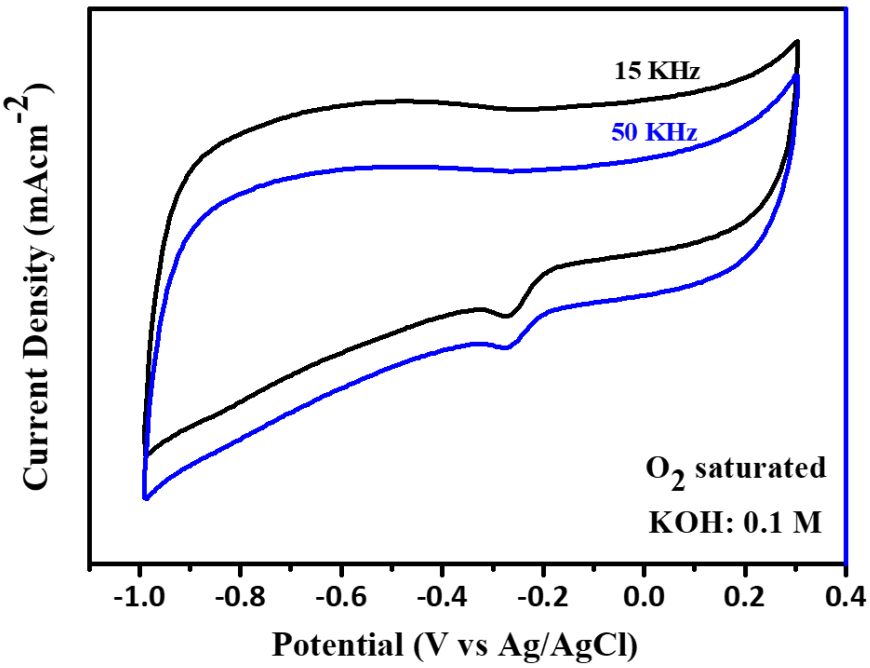

Fig. 2-8 Electrochemical measurements of CV curves of nanocarbon of low 15 KHz and High 50 KHz frequencies under O_2 saturated 0.1 M KOH solution at a scan rate of 50 mVs^{-1}.

2.4. Summary

Palm oil is an available bioresource and relatively lower cost for nanocarbon synthesis. The obtained carbon materials have various kinds of applications, such as adhesives, paints, printing inks, surface coatings and composite preparation. We were successfully synthesised nanocarbon materials from palm oil by spp. The frequencies were able to effects on the carbon yield (%), crystallinity and morphology. When the frequencies were increased, the amount of carbon also increased with them. Currently, SPP is widely accepted in the synthesis of nanocarbon materials within a short time with room temperature and atmospheric pressure and produced a high % of yield. However, the yield of carbon and synthesis rate was quite smaller than organic solvent. Furthermore, the nanocarbon had an ORR activity with high electrical conductivity by SPP.

References

1) G. Wang, G. Sun, Q. Wang, S. Wang, H. Sun, and Q. Xin, Int. J. Hydrog. Energy, 35, 11245-11253 (2010).

2) A. B. Suriani, A. Aziz, S. F. Nik, R. M. Nor, and M. Rusop, Mater. Lett., *63*, 2704-2706 (2009).

3) R. Kumar, R. K. Singh, and D. P. Singh, Renew. Sustain. Energy Rev., 58, 976-1006 (2016).

4) J. K. Sudesh, K. Bhubalan, J. A. Chuah, Y. K. Kek, H. Kamilah, N. Sridewi, and Y. F. Lee, Appl. Microbiol. Biotechnol., *89*, 1373-1386 (2011).

5) Y. Xia, and R. C. Larock, Green Chem., 12, 1893-1909 (2010).

6) G. Lligadas, J. C. Ronda, M. Galia, and V. Cadiz, Mater. Today, 16, 337-343 (2013).

7) C. S. Lee, Y. Ju, S. Shim, J. Kim, and T. H. Kim, J. Biomed. Nanotechnol., 15, 2321-2331 (2019).

8) S. Mekhilef, S. Siga, and R. Saidur, Renew. Sust. Energ. Rev., 15, 1937-1949 (2011).

9) X. Fu, X. Fu, W. Li, Y. Chen, and Z. Cai, J. Biomed. Nanotechnol. 15, 1232-1240 (2019).

10) M. Z. Islam, S. Arata, K. Hayashi, A. Kobayashi, and K. Niitsu, Nanosci. Nanotechnol. Lett., 12, 101-106 (2020).

11) S. Chae, K. Hashimi, M. A. Bratescu, and N. Saito, Nanosci. Nanotechnol. Lett., 10, 784-789 (2018).

12) N. Saito, J. Hieda, and O. Takai, Thin Solid Films, 518, 912-917 (2009).

13) Z. Chen, Y. Bai, F. Zhao, L. Cao, G. Han, and Y. Yin, J. Biomed. Nanotechnol. 15, 930-938 (2019).

14) L. Wu, H. Tang, H. Zheng, X. Liu, Y. Liu, J. Tao, Z. Liang, Y. Xia, and Y. Xu, J. Biomed. Nanotechnol. 15, 138-150 (2019).

15) J. Luo, H. Kong, M. Zhang, J. Cheng, Z. Sun, W. Xiong, Y. Zhu, Y. Zhao, and H. Qu, J. Biomed. Nanotechnol. 15, 151-161 (2019).

16) A. Aljaafari, and S. S. Ibrahim, Mater. Express 9, 872-881 (2019).

17) N. Zhuang, J. Chen, M. Zheng, and D. Chen, Mater. Express 9, 923-930 (2019).

18) X. Zhang, X. Gan, Y. Liu, M. Xie, and J. Yi, Mater. Express 9, 648-652 (2019).

19) N. Dongmulati, X. Maimaitiyiming, and Y. Maimaiti, Mater. Express 9, 281-290 (2019).

20) Y. Zhang, Y. Cheng, T. Zhang, B. Wang, and H. Xiao, Mater. Express 9, 213-225 (2019).

21) Q. Yang, M. Wang, Y. Sun, S. Peng, and Y. Cao, Chin. Chem. Lett., 30, 1224-1228 (2019).

22) Y. Lai, C. Zhang, Y. Deng, G. Yang, and N. He, Chin. Chem. Lett., 30, 160-162 (2019).

23) A. Watthanaphanit, and N. Saito, *Jpn. J. Appl. Phys.*, 57, 0102A3-10 (2018).

24) O. Takai, Pure Appl. Chem., 80, 2003-2011 (2008).

25) S. Chae, G. Panomsuwan, M. A. Bratescu, K. Teshima, and N. Saito, ACS Appl. Nano Mater., 2, 1350-1355 (2019).

26) K. Wang, Q. Shi, Q. Ji, H. Li, D. Zhang, H. Feng, and H. Fan, J. Biomater. Tissue Eng. 8, 1719-1724 (2018).

27) P. Brault, A. Caillard, A. L. Thomann, J. Mathias, C. Charles, R. W. Boswell, S. Escribano, J. Durand, and T. Sauvage, J. Phys. D Appl. Phys., 37, 3419-3423 (2004).

28) H. Rabat, and P. Brault, Fuel Cells 08, 81-86 (2008).

29) S. Lee, H. K. Baik, J. Yoo, and J. H. Han, Diam. Relat. Mater., 11, 914-917 (2002).

30) P. Meeprasertsagool, A. Watthanaphanit, T. Ueno, N.Saito, and P. Reubroycharoen, Energy Procedia 138, 1153-1158 (2017).

31) O. Takai, J. Photopolym. Sci. Technol., 27, 379-384 (2014).

32) N. Saito, M. A. Bratescu, and K. Hashimi, Jpn. J. Appl. Phys., 57, 0102A4 (2018).

33) N. Saito, T. Ueno, M. A. Bratescu, and J. Hieda, Novel Structured Metallic and Inorganic Materials, 343-355 (2019).

34) A. Watthanaphanit, G. Panomsuwan, and N. Saito, RSC Advances, 4, 1622-1629 (2014).

35) T. Sudare, T. Ueno, A. Watthanaphanit, and N. Saito, J. Phys. Chem. A, 119, 11668-11673 (2015).

36) S. Nemoto, T. Ueno, A. Watthanaphanit, J. Hieda, M. A. Bratescu, N. Saito, Jpn. J. Appl. Phys., 56, 096202 (2017).

37) A. S. Ismail, A. H. Shukker, and A. A. Fayad, Energy Procedia 141, 315-331 (2017).

38) L. G. Cancado, K. Takai, and T. Enoki, Appl. Phys. Lett., 88, 163106 (2006).

39) R. Saito, M. Hofmann, G. Dresselhaus, A. Jorio, and M. S. Dresselhaus, Adv. Phys., 60, 413-550 (2011).

40) E. Frackowiak, and F. Béguin, Carbon 39, 937–950 (2001).

Chapter 3

Nanocarbons-encapsulated WC synthesized by solution plasma process in palm oils with high frequency discharges

Chapter 3 - Nanocarbons-encapsulated WC synthesized by solution plasma process in palm oils with high frequency discharges

3.1. Introduction

Tungsten carbide (WC) has attractive properties like high electrical conductivity, CO and corrosion resistance. [1-2] It is the non-noble metals and able to perform the catalytic activity. The WC can be enhanced with the nanocarbon materials due to their special properties, such as conductivity, electrocatalytic activity, mechanical capacity and chemical and thermal existence. [3-6] Nanocarbon has been used as electrode materials in a fuel cell, rechargeable lithium batteries, catalyst support, supercapacitor electrode and organic solar cells. [7-13] Nanocarbon materials have been developed fullerenes, carbon nanotubes and onions. [14-24] It has been encapsulated in graphitic nanocages and nanotubes by conventional arc-discharge. [25, 26] Nanocarbons-encapsulated WC is interesting due to core-shell like structure. [27-29] The core-shell nanostructures were synthesized from polymers and silica. Previously, nanocarbon has been encapsulated from organic solvent. [30-32] In this work, we are synthesized Nanocarbons-encapsulated WC from palm oil. Recently, palm oil is used in a fuel cell, bio-based polymers, liquid hydrocarbon fuels and biodiesel. [33-35] The advantages of palm oil consist of low toxicity, chemically inert, inherent biodegradability, and global sustainability. [36, 37] The key point of palm oil is constituted by triglyceride (95 - 98%) and minor compounds as mono- and diglycerides (2 - 5%). Triglycerides contain three molecules such as saturated fatty acids, unsaturated fatty acids, and glycerol. [38] The saturated fatty acids have only a carbon-carbon

single bond, and the unsaturated fatty acids contain many carbon-carbon double or triple bonds. Fatty acid composition of palm oil is palmitic acid ($C_{16}H_{32}O_2$, 39%), oleic acid ($C_{18}H_{34}O_2$, 45%), linoleic acid ($C_{18}H_{32}O_2$, 9%), stearic acid ($C_{14}H_{28}O_2$, 5%), and others (2%).[39] The encapsulated carbons were investigated by conventional technics such as arc discharge, chemical vapour deposition, microwave heating, thermal plasma processing and pyrolysis. However, thus technic has limitation due to a long time, multiple steps and high energy consumption. To overcome this problem, the nanocarbons-encapsulated WC were synthesized by Solution plasma process (SPP).[40-46] SPP has many advantages such as simple experimental setup, short time and room temperature and atmospheric pressure. The more advantage of SPP able to synthesis the nanomaterials without any catalyst.

In this research, the nanocarbons-encapsulated WC was synthesized by SP in the palm oil. The structural and properties characterization of the synthesized materials obtained were encapsulated in onion-like nanocarbon shells and the average size diameters 4-12 nm. The electrochemical properties are showed the nanocarbon entirely encapsulated with WC. The synthesized nanocarbons-encapsulated WC might be applied in data storage and energy applications.

3.2. Experimental procedure

In this study, Palm oil (Kobe Busan Co., Ltd. Japan) (100% vegetable cooking oil) was selected as a material of 200 ml for the nanocarbon-encapsulated WC synthesis as shown in Fig. 3-1. A bipolar pulsed power supply (KURITA Seisakusho, Japan) applied two tungsten (W) electrodes (wire type, purity 99.9%, The Nilaco Corporation, Japan) with a 1 mm diameter covered the ceramic tube with 0.5 mm electrode gap into the palm oil in a closed system vessel. The repetition frequencies (100, 150, and 180 kHz) are used at 2 μs pulse widths for 30 min. The electrodes were adjusted several times to keep a constant gap distance between the

electrodes, due to erosion. When the electrode gap distance was increased from 0.5 mm to 1 mm or more, the discharge stops. After synthesis of the nanocarbon materials, the liquid and solid phase were separated by centrifugation. The solid phase was washed three times with acetone until the oils have been fully removed using centrifugation at 12000 rpm for 30 min and then dried at 90ºC for 6 hours in an oven (DX301, Yamato Co. Ltd., Japan). This balance (EK2000i, AS-ONE Co. Ltd., Japan) used for a weight of nanocarbon. The structural properties were using X-ray diffraction (XRD, Rigaku Smart lab, Rigaku Corporation, Japan) with a Cu Kα as X-rays radiation at λ = 0.154 nm in the 2Θ range from 3.0 to 90.0 degrees and a scan speed of 3.0 degrees. Raman spectroscopy (NRS-100, JASCO Corporation, Japan) used a laser with a wavelength of 532.5 nm and 1 mW power to determine the type of nanocarbon material. The X-ray Photoelectron Spectroscopy (XPS, PHI 5000 Versa Probe II; Ulvac-Phi physical Electronics INC, Japan) measured the elemental composition using the Mg Kα X-ray source with an energy of the photon of 1253.6 eV. The morphologies of structure, shape, and size were viewed by Transmission electron microscopy (TEM, JEM-2500SE, JEOL Ltd., Japan) at 200 kV for the synthesized nanocarbon. The electrochemical activity was determined by measuring the cyclic voltammetry (CV, HZ5000, Hokuto Denko Inc., Japan) using a conventional three-electrode cell setup with the glassy carbon (GC) electrode (with 3 mm disk diameter) as the working electrode, a platinum wire as the counter electrode, and an Ag/AgCl electrode in saturated KCl as reference. The catalyst ink was prepared as follows: 10.0 mg of WC-nanocarbon was dispersed into 2 ml ethanol and 150 µL Nafion® by ultrasonication for 20 min. The homogeneous ink was dropped on the GC electrode until fielded and dried at room temperature. The used electrolyte was 0.5 M H2SO4 (Kanto Chemical Co., Inc., Japan) saturated with O_2. The scan rates were 50 mV s^{-1}, the scan range was from -0.2 to 1.2 V, with a sampling rate of 100 ms.

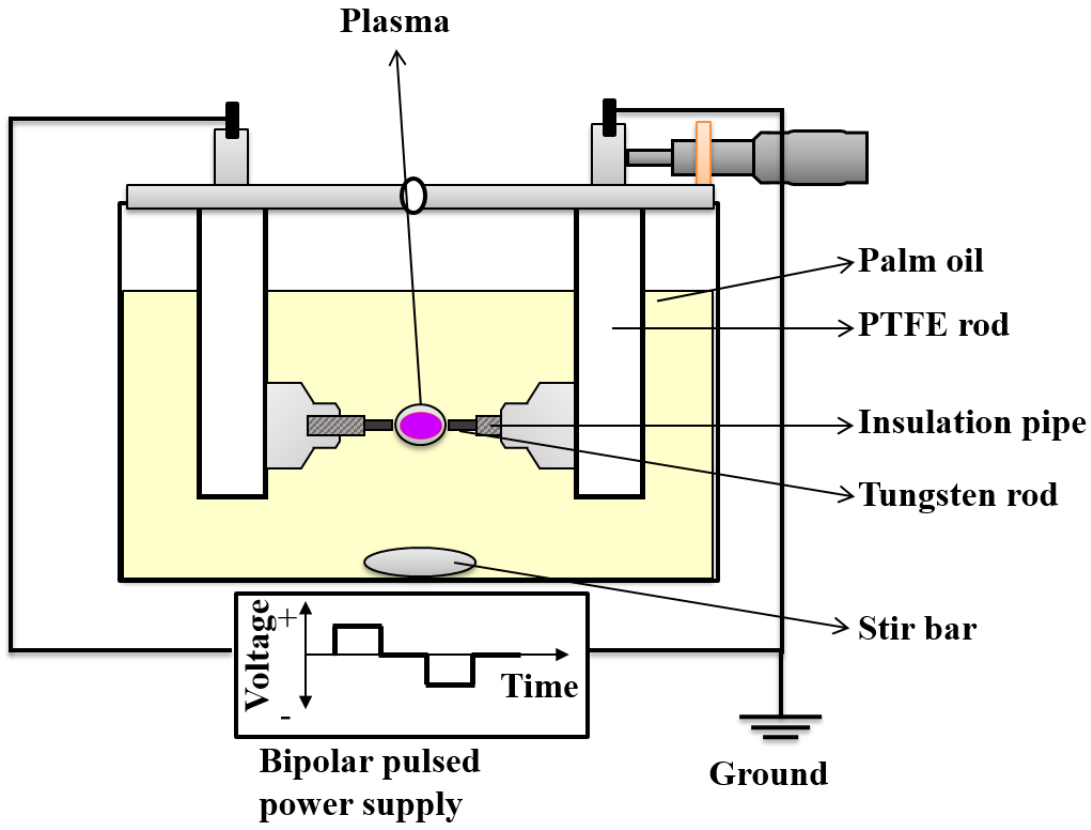

Fig. 3-1 Schematic diagram of nanocarbon-encapsulated WC by SP in palm oil.

3.3. Results and discussion

3.3.1. *Structural properties*

XRD shown in Fig. 3-2 characterized the structural properties of nanocarbons-encapsulated WC. The nanocarbons peaks at 23.5° and 42.3° were the reflections at 0 0 2 and 1 0 1 planes (JCPDS 75-1621). [42-44] When increased the frequencies, the peaks of 0 0 2 reflections also sharply increased with them. In the case of 100 kHz frequency, the XRD peak is broader at 0 0 2 corresponding 150 and 180 kHz frequencies are showed the sharp peak due to the high frequency from the power supply. The reflections of WC (JCPDS #25-1047) peaks were identifications in the 100, 150 and 180 kHz

corresponded to the 111, 200, 220, 311, and 222 planes. [47, 48] These results indicate that SP in palm oil synthesized the nanocarbons-encapsulated WC contains amorphous structure at 100 kHz frequency and amorphous-like turbostratic structure at 150 and 180 kHz frequencies.

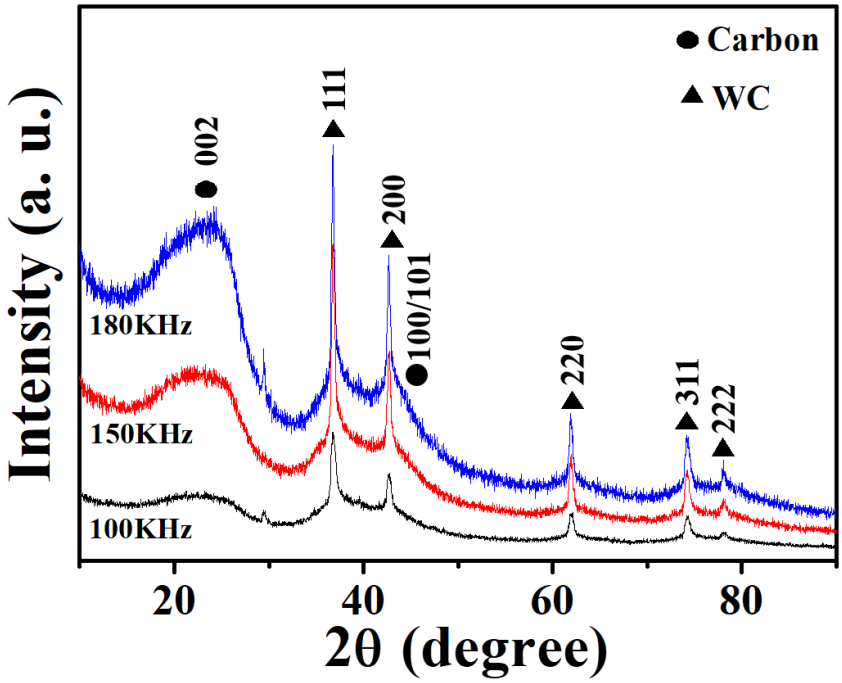

Fig. 3-2 XRD patterns of nanocarbon-encapsulated WC by SP in palm oil at 100, 150 and 180 kHz frequencies in 2μs for 30 min discharge.

Raman spectroscopy showed that the D and G bands were observed the peaks at 1350 and 1580 cm^{-1}. Structural disorder and sp^2 graphite sheet-like structure were respectively obtained from D and G band. The I_D/I_G ratio for the nanocarbon using different plasma frequencies 100, 150 and 180 kHz respectively 1.01, 1.00 and 0.99 calculated from peak heights as shown in Fig. 3-3. The D/G ratio decreased with pulse frequency. For results, the number of sp^2 in nanocarbon increased and its core-shell structure and bond disordering. The 2D peak at 2600–2750 cm^{-1}, it confirms that WC-

nanocarbon has a quite high degree of crystallinity as well as nanocarbon. Raman showed crystallite sizes $L_{a,}$ and the ratio I_D/I_G was inversely proportional to the crystallite sizes L_a, where laser energy E_1 and wavelength λ= 532 nm, the equation is L_a (nm) = (2.4x 10^{-10}) λ^4 $(I_D/I_G)^{-1}$ [49, 50]. The crystallite sizes L_a (nm) was increased (19.0 to 19.4 nm) with increase the frequency. These results indicate that when increasing the frequency, then WC-nanocarbon crystallinity also increases.

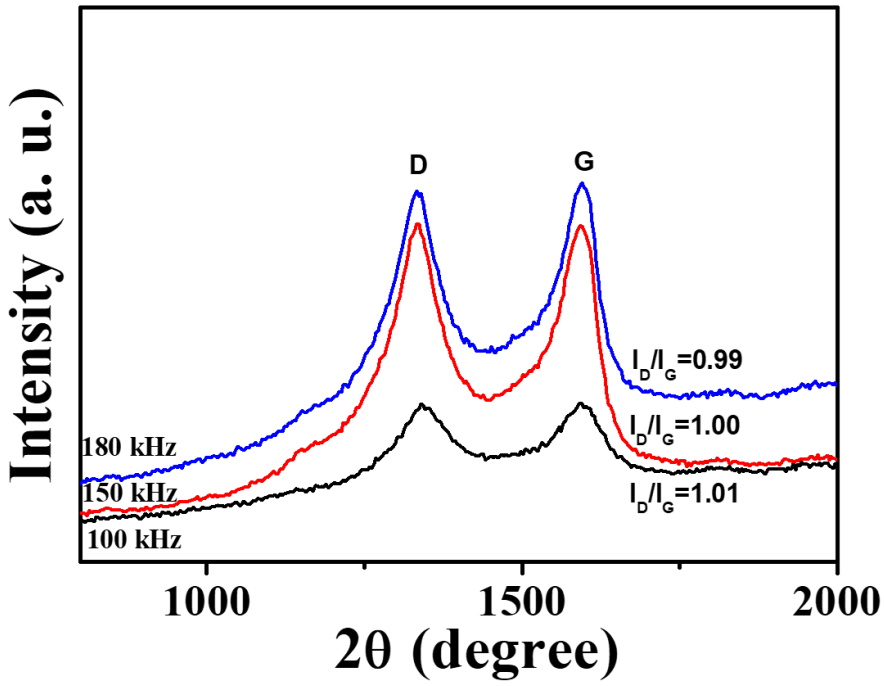

Fig. 3-3 Raman spectra of WC-nanocarbon from palm oil at various frequencies 100, 150 and 180 kHz in 2 μs at 30 min discharge.

3.3.2. *Morphology*

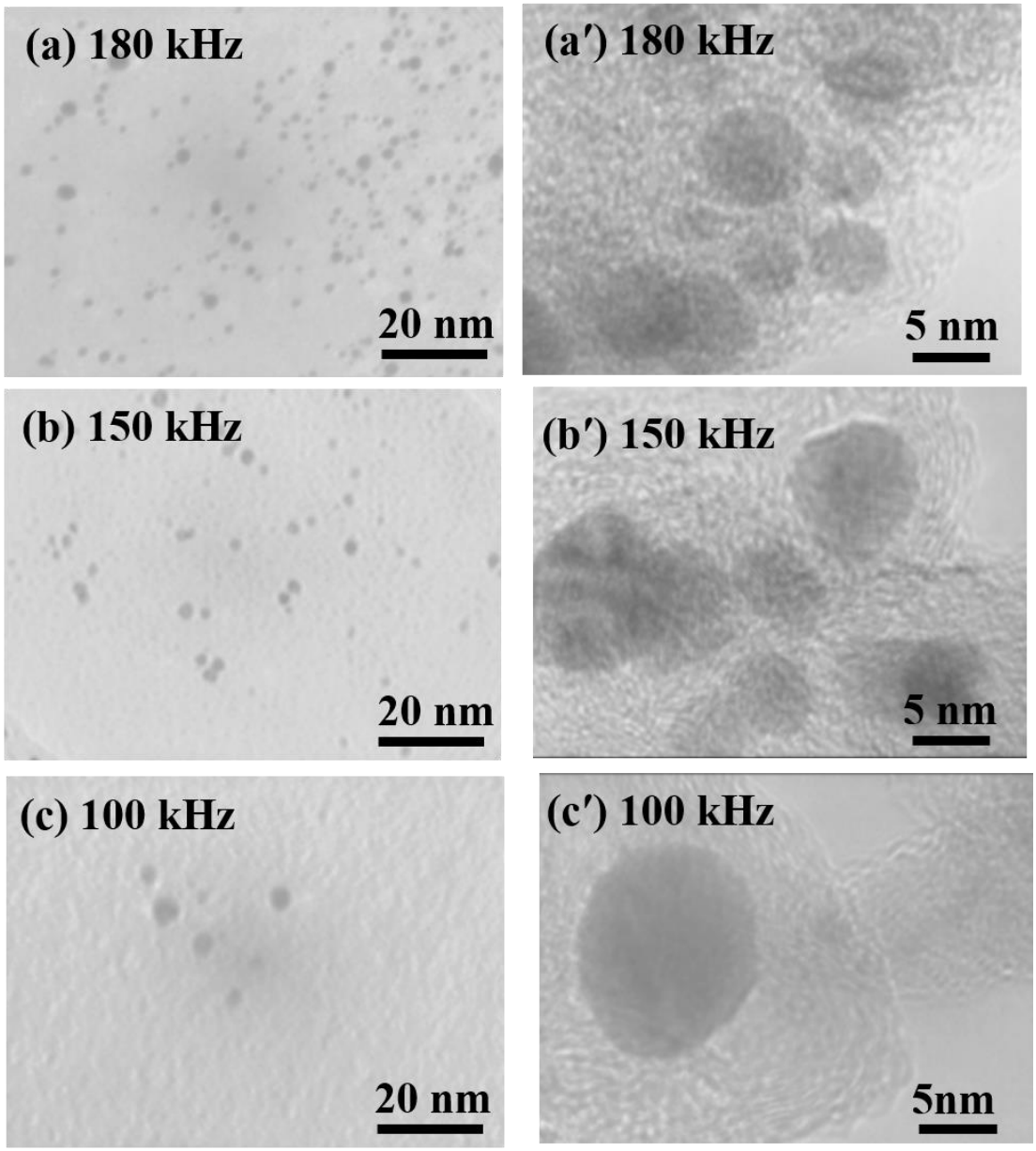

Fig. 3-4 TEM images of nanocarbons-encapsulated WC correspond with HR-TEM and SEAD pattern (insert) from palm oil, (a, a′ and a″) 100 kHz; (b, b′ and b″) 150 kHz; and (c, c′ and c″) 180 kHz of 2 μs at 30 min discharge.

The morphology of nanocarbons-encapsulated WC was observed using the TEM at Fig. 3-4 a), b) and c) and high-resolution TEM (HR-TEM) at Fig. 3-4 a′), b′) and c′). The TEM images show that the observed nanocarbons-capsulated WC indicator spherical shapes and core-shell

like morphology. When increased the frequencies 100, 150 and 180 kHz, the nanocarbons-encapsulated WC size decreased. The 180 kHz frequency showed the narrow capsule size distributions compared with 100 and 150 kHz. The HR-TEM showed that obtained nanocarbons-encapsulated WC uniform sizes 4-12 nm and completely nanocarbons encapsulated with WC. In the case of 100 kHz of HR-TEM at Fig. 3-4 c′) the image indicates that the nanocarbons capsulated well and an average size of 12 nm. Also, the 150 and 180 kHz frequencies of HR-TEM images were showed the obtained nanocarbons encapsulated like core-shell structure and average size distribution respectively 7 nm and 4 nm, its less than 100 kHz frequency. These results indicate that the frequencies able to effect on the nanocarbons-encapsulated WC morphology like shapes and size. The morphology of the nanocarbon-encapsulated WC observed the spherical shapes in all frequencies.

3.3.2. *ORR activity*

The nanocarbons-encapsulated WC by SP in palm oil applied high frequencies 100, 150 and 180 kHz at 2 μs. The CV curve of all conditions of nanocarbons-encapsulated WC was analysed in an acid medium 0.5 M H_2SO_4 solution under O_2 saturated with scan rate 50 mVs^{-1} in Fig. 3-5. The potential range is –2.0 to 1.2 V and a current density range is -3.0 to 4.0 $mAcm^{-2}$. As a result of 100 kHz frequency under O_2 saturated, the cathodic (oxygen reduction reaction, ORR) peak at 0.32 V and the onset potential was observed at 0.61 at 50 scan rate. Also, when increased the frequencies from 150 and 180 kHz, the ORR peak was gradually disappeared. This results indicated that the nanocarbon was encapsulated WC because it would not exhibit any ORR peaks during the measurement of CV. The CV results indicated that when the frequencies were increased, the ORR peaks also gradually decreased and the encapsulated nanocarbon also increased.

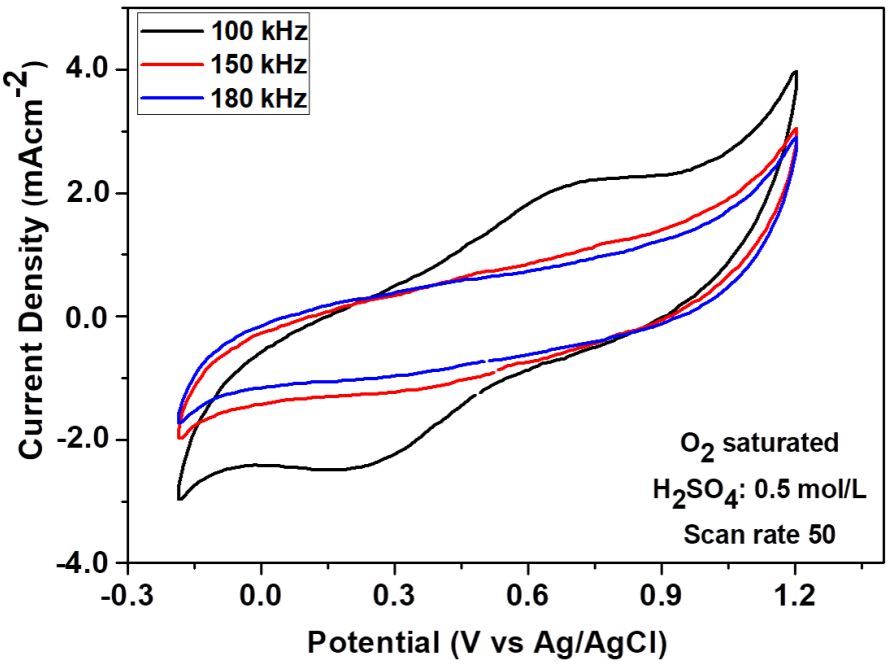

Fig. 3-5 Electro-catalytic activity CV for 100, 150 and 180 kHz frequencies at 2 µs of nanocarbons-encapsulated WC in 0.5 mol/L H_2SO_4 under O_2-saturated and scan rate 50 mV/s.

3.4. Summary

In conclusion, the nanocarbon-encapsulated WC were synthesized by SP in palm oil using at different frequencies effective on morphology and structure and ORR activity. When the frequencies were increased, the nanocarbon-encapsulated WC of % yield and synthesis rate also increased as shown in table 1. In the case of 180 kHz frequency, the highest synthesized rate was 3.07 mg/min. Currently, SPP is widely accepted in the synthesis of nanocarbon materials within a short time with room temperature and atmospheric pressure and produced a high % of yield. The potential of nanocarbon-encapsulated WC by SP in the palm oil would be helpful for the next generation.

References

1) R. Venkataraman, H. R. Kunz, and J. M. Fenton, J. Electrochem. Soc., 150, A278-A284 (2003).
2) S. T. Oyama, Catal. Today, 15, 179-200 (1992).
3) P. M. Ajayan, Chem. Rev., 99, 1787−1799 (1999).
4) G. Panomsuwan, A. Watthanaphanit, T. Ishizaki, and N. Saito, Phys. Chem. Chem. Phys., 17, 13794-13799 9201 (2015).
5) Z. O. Malaibari, Mater. Express, 9, 85–98 (2019).
6) T. Ishizaki, S. Chiba, Y. Kaneko, and G. Panomsuwan, J. Mater. Chem. A, 2, 10589-10598 (2014).
7) J. Kang, O. L. Li, and N. Saito, Nanoscale 5, 6874-6882 (2013).
8) Y. Liu, L. Wei, L. Liao, S. Chen, K. Zhang, and A. Qin, Mater. Express, 9, 112–122 (2019).
9) K. Wang, J. Xu, H. Li, X. Wang, Y. Wu, D. Zhang, H. Feng, and H. Fan, J. Biomater. Tissue Eng., 8, 309–316 (2018).
10) K. Wang, Q. Shi, Q. Ji, H. Li, D. Zhang, H. Feng, and H. Fan, J. Biomater. Tissue Eng., 8, 1719–1724 (2018).
11) P. Premphet, K. Leksakul, J. X. Piao, S. B. Jin, P. Pothacharoen, R. Supruangnet, and D. Boonyawan, J. Biomater. Tissue Eng., 8, 824–828 (2018).
12) S. Y. Son, J. M. Yun, Y. J. Noh, S. Lee, H. N. Jo, S. I. Na, and H. I. Joh, Carbon, 81, 546-551 (2015).
13) S. A. Ansari, N. Parveen, T. H. Han, M. O. Ansari, and M. H. Cho, Phys. Chem. Chem. Phys., 18, 9053-9060 (2016).
14) M. Z. Islam, S. Arata, K. Hayashi, A. Kobayashi, and K. Niitsu, Nanosci. Nanotechnol. Lett., 12, 101-106 (2020).

15) Y. Liu, L. Wei, L. Liao, S. Chen, K. Zhang, and A. Qin, Mater. Express, 9, 112–122 (2019).

16) Q. Yang, M. Wang, Y. Sun, S. Peng, and Y. Cao, Chin. Chem. Lett., 30, 1224-1228 (2019).

17) Z. Li, T. Liu, J. Long, Y. Wu, and Y. Cao, Chin. Chem. Lett., 30, 582-586 (2019).

18) Y. Lai, C. Zhang, Y. Deng, G. Yang, and N. He, Chin. Chem. Lett., 30, 160-162 (2019).

19) Q. Sun, L. Liu, Y. Yang, Z. Zha, and Z. Wang, Chin. Chem. Lett., 30, 1379-1382 (2019).

20) C. –S, Lee, Y. Ju, S. Shim, J. Kim, and T. H. Kim, J. Biomed. Nanotech., 15, 2321–2331 (2019).

21) X. Fu, X. Fu, W. Li, Y. Chen, and Z. Cai, J. Biomed. Nanotech., 15, pp.1232–1240 (2019).

22) Z. Chen, Y. Bai, F. Zhao, L. Cao, G. Han, and S. Yin, J. Biomed. Nanotech., 15, 930–938 (2019).

23) L. Wu, H. Tang, H. Zheng, X. Liu, Y. Liu, J. Tao, Z. Liang, Y. Xia, Y. Xu, Y. Guo, H. Chen, and J. Yang, J. Biomed. Nanotech., 15, 138–150 (2019).

24) R. Tenne, L. Margulis, M. Genut, and G. Hodes, Nature, 360, 444–446 (1992).

25) P. Meeprasertsagool, A. Watthanaphanit, T. Ueno, N. Saito, and P. Reubroycharoen, Energy Procedia 138, 1153-1158 (2017).

26) P. M. Ajayan, O. Stephan, P. Redlich, and C. Colliex, Nature, 375, 564–567 (1995).

27) P. Chaiyasat, P., M. Z. Islam, and A. Chaiyasat, RSC Adv., 3, 10202–10207 (2013).

28) P. Q. Phan, S. Chae, P. Pornaroontham, Y. Muta, K. Kim, X. Wang, N. and Saito, RSC Adv., 10, 36627–36635 (2020).

29) S. Namwong, M. Z. Islam, S. Noppalit, P. Tangboriboonrat, P. Chaiyasat, and A. Chaiyasat, J. Macromol. Sci. A, 53, 11-17 (2016).

30) N. Saito, J. Hieda, O. Takai, Thin Solid Films, 518, 912-917 (2009).

31) A. Watthanaphanit, and N. Saito, Jpn. J. Appl. Phys., 57, 0102A3 (2018).

32) N. Saito, M. A. Bratescu, K. Hashimi, Jpn. J. Appl. Phys., 57, 0102A4 (2018).

33) G. Mehta, A. K. Mohanty, M. Misra, and L. T. Drzal, Green Chem., 6, 254-258 (2004).

34) M. Z. Islam, A. Watthanaphanit, S. Chae, and N. Saito, Nanosci. Nanotechnol. Lett., accepted (2020)

35) N. Taufiqurrahmi, and S. Bhatia, Energy Environ. Sci., 4, 1087-1112 (2011).

36) Y. Xia, and R. C. Larock, Green Chem., 12, 1893–1909 (2010).

37) G. Lligadas, J. C. Ronda, M. Galia, and V. Cadiz, Mater. Today, 16, 337-343 (2013).

38) T. Murphy, R. Hayes, S. Imberti, G. G. Warr, and R. Atkin, Phys. Chem. Chem. Phys., 16, 13182-13190 (2014).

39) K. F. Adekunle, Open J. Polym. Chem., 5, 34-40 (2015).

40) O. Takai, Pure Appl. Chem., 80, 2003-2011 (2008).

41) N. Saito, N., T. Ueno, M. A. Bratescu, and J. Hieda, Novel Structured Metallic and Inorganic Materials, 343-355 (2019).

42) A. Watthanaphanit, G. Panomsuwan, and N. Saito, RSC Adv., 4, 1622–1629 (2014).

43) S. Chae, K. Hashimi, M. A. Bratescu, and N. Saito, Nanosci. Nanotechnol. Lett., 10, 784-789 (2018).

44) S. Chae, G. Panomsuwan, M. A. Bratescu, K. Teshima, and N. Saito, ACS Appl. Nano Mater., 2, 1350−1355 (2019).

45) T. Sudare, T. Ueno, A. Watthanaphanit, and N. Saito, J. Phys. Chem. A., 119, 11668−11673 (2015).

46) S. Nemoto, T. Ueno, A. Watthanaphanit, J. Hieda, M. A. Bratescu, and N. Saito, Jpn. J. Appl. Phys., 56, 096202 (2017).

47) M. Matsumoto, Y. Saito, C. Park, T. Fukushima, and T. Aida, Nat. Chem., 7, 730−736 (2015).

48) L. Liu, Z. Xiong, D. Hu, G. Wu, and P. Chen, Chem. Comm., 49, 7890−7892 (2013).

49) A. Ferrari, J. Meyer, V. Scardaci, C. Casiraghi, M. Lazzeri, F. Mauri, S. Piscanec, D. Jiang, K. Novoselov, and S. Roth, Phys. Rev. Lett., 97, 187401 (2006).

50) A. C. Ferrari, J. Robertson, Phys. Rev. B, 61, 14095-14107 (2000).

Chapter 4

Nitrogen, Oxygen and Tungsten containing nanocarbons by solution plasma process for fuel cell and Li-air battery applications

Chapter 4 - Nitrogen, Oxygen and Tungsten containing nanocarbons by solution plasma process for fuel cell and Li-air battery applications

4.1. Introduction

Recently, Li-air batteries have been largely used in energy conversion and storage devices for various applications. [1-4] These face the critical challenges that from poor cycle life, low practical energy density, low round-trip efficiency, and high manufacturing costs. To improve the energy storage properties, catalytic activity and less cost, the ORR are demanded. [5–7]

Presently, platinum (Pt) is commonly used as a catalyst for ORR but their high cost of the production and long term instability. [8–10] To introduce the alternatives of Pt catalysts, the nanocarbons and heteroatom-doped nanocarbon are attracted. The advantages of the nanocarbons and the heteroatom-doped nanocarbon are the low production cost, excellent chemical properties and the higher electrical conductivity. [11, 12]

The nanocarbons such as carbon black, carbon nanotubes, porous and nonporous carbon materials and graphene are showed large specific surface area, high conductivity, electrocatalytic activity, mechanical capacity, ultra-light characteristics, and chemical and thermal resistance.[13–18] In heteroatom (nitrogen, boron, and phosphorus) doped nanocarbon are showed the higher ORR activity. [19–23]

Previously, the nanocarbon materials were successfully synthesized by catalytic or noncatalytic chemical vapor deposition, pyrolysis, electric arc discharge, and direct-current

(DC) discharge plasma from various organic solvents. [24–29] However, these synthesis technique are complicated due to their high process temperatures, low production yield, and the possing time. [30–33]

Recently the energy saving and a non-equilibrium liquid phase plasma named Solution Plasma Process (SPP) are used to synthesize nanocarbon materials at room temperature. [34–38] In our laboratory, we conducted various experiments to produce carbon materials from organic solvents by SPP. [39–42]

In this research, the synthesis of nanocarbons by SPP with differences frequencies and pulse widths at electrode distance of 0.75 mm for 30 min. The synthesis rate is the main target to the synthesis of nanocarbons with their electrocatalytic activity (such as Li-air battery and fuel cell) without thermal treatment and the commercial Pt/C catalyst. The catalytic activity of ORR were obtained in acidic medium. The crystallinity, structure, surface area, morphology, elemental composition, electrical conductivity, ORR activity and Li-air battery were investigated from nanocarbons. In the case of Li-air battery, N containing nanocarbons (Nanocarbons of BZ-NH_2) were obtained a high special capacity of 15500 mAh/g carbon compare with the nanocarbon of palm oils.

4.2. Experimental procedure

4.2.1 *Materials*

Benzene (>99%; Kanto Chemical Co., INC, Japan), Nitrobenzene (>99%; Kanto Chemical Co., INC, Japan) Aniline (>99%; Kanto Chemical Co., INC, Japan), Polyvinylidene Fluoride (PVDF, Sigma-Aldrich, Japan), N-Methyl-2-pyrrolidone (NMP, Kanto Chemical Co., INC, Japan), Acetone (Kanto Chemical Co., INC, Japan) and Ethanol (Kanto Chemical Co., INC, Japan) were purchased.

4.2.2 *Experimental setup and production procedure*

The experimental setup of SPP is shown in Fig. 4-1. The plasma was generated by a bipolar pulsed power supply (MPS-R06K01C-WP1-6CH, Kurita Co. Ltd., Japan) between two tungsten (W) electrodes (wire type, purity 99.9%, The Nilaco Corporation, Japan) with a 1 mm diameter, covered with an insulating ceramic tube. The electrode gap was 0.75 mm in the beginning. The concentration of BZ, BZ-NO_2, and BZ-NH_2 are 50, 18, and 50 mg/L, respectively. The applied high voltage had different pulse widths (0.5, 1.0 and 2 μs) and repetition frequencies (50, 100, and 150 kHz). The process time was 30 min. The current and voltage waveforms were observed using an oscilloscope (DLM 2022, Yokogawa Meters & Instruments Corporation, Japan) in the range of 0 – 5 A and 0.6 - 1.0 kV, respectively. During SPP, the electrodes were adjusted several times, especially at high frequencies of SPP operation (*i.e.,* 100 and 150 kHz) to keep a constant gap distance between the electrodes. Due to erosion, the electrode gap distance increases. This adjustment also has the role in maintaining a stable plasma during the process. If the electrode gap distance increases from 0.75 mm to 1 mm or more, the discharge stops. After the nanocarbon materials synthesis, the remained liquid and solid phases were separated by filtration then dried at 90ºC for five hours in an oven (DX301, Yamato Co. Ltd., Japan). The weight of nanocarbon was measured using a balance (EK2000i, AS-ONE Co. Ltd., Japan). The carbon yield (Y in %) and synthesis rate (R in mg/min) were calculated from the amount of carbon powders as:

$$Y = (M/M_0) \times 100$$

where M is the mass of the carbon powder, and M_0 is the initial mass of BZ, BZ-NO2 and BZ-NH2. However, the synthesis rate was calculate as R= M/T. Where T is total process time (i.e., 30 min).

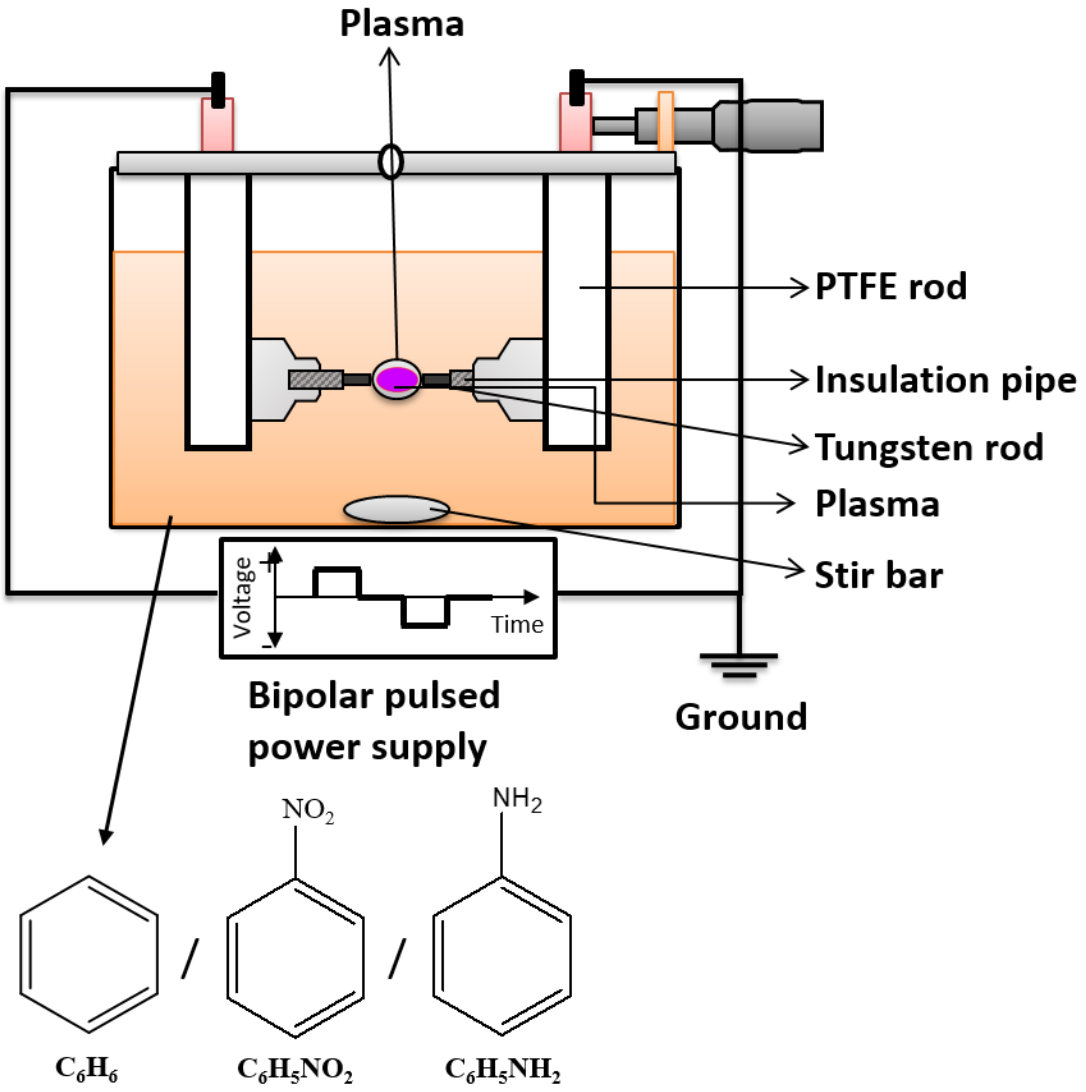

Fig. 4-1 Schematic diagram of experimental setup with BZ, BZ-NO_2 and BZ-NH_2 of precursors for solution plasma process (SPP).

4.2.3. *Characterization*

The structural properties were investigated by X-ray diffraction (XRD, Rigaku Smart lab, Rigaku Corporation, Japan) with a Cu Kα X-ray radiation source at λ = 0.154 nm in the 2Θ range from 3.0 to 90.0 degrees and a scan speed of 3.0 degrees; and Raman spectroscopy (NRS-100, JASCO Corporation, Japan) used a laser with the wavelength of 532.5 nm and 1 mW power to determine the type of nanocarbons. The morphology, shape, and size of nanocarbons

were observed by Transmission electron microscopy (TEM, JEM-2500SE, JEOL Ltd., Japan) with an electron gun at 200 kV. The surface area, pore volume, and average pore diameter were observed by Brunauer-Emmett-Teller (BET, BELSORP-mini-II, BEL JAPAN, INC, Japan) from the nitrogen adsorption-desorption isotherms at 77 K. The elemental compositions were observed by X-ray Photoelectron Spectroscopy (XPS, PHI 5000 Versa Probe II; Ulvac-Phi physical Electronics INC, Japan) using the Mg Kα X-ray source with an energy of the photon of 1253.6 eV. The electrical resistivity and electrical conductivity were determined by a four-point probe method (Laresta-GP, MCP-T610, Mitsubishi Chemical Analytech Co., Ltd., Japan). A concentration of 60 wt% of nanocarbons was mixed with 40 wt% polymer binder (PVDF) and then sonicated in NMP during 30 min. The emulsion was dropped on a glass substrate, then dried in an electric oven at 120^{o} C for 20 min to form a uniform film.

4.2.3. *Electrochemical measurement*

The cyclic voltammetry (CV) measurement was connected a computer-controlled ALS-CH model 704 ES electrochemical analyzer (CH instrument Inc.). The ink made by catalyst (5.0 mg), ultrapure water (480 mL), ethanol (480 mL), and Nafion® aqueous solutions (40 mL) were ultra-sonicated was obtained. The Ag/AgCl solution was applied as the counter and reference electrodes at 0.5 mol/L H_2SO_4 electrolyte under N_2 and O_2 gas saturated. The scan rate is 20 mVs^{-1} at –0.2 V to 1.2 V (V vs. Ag/AgCl).

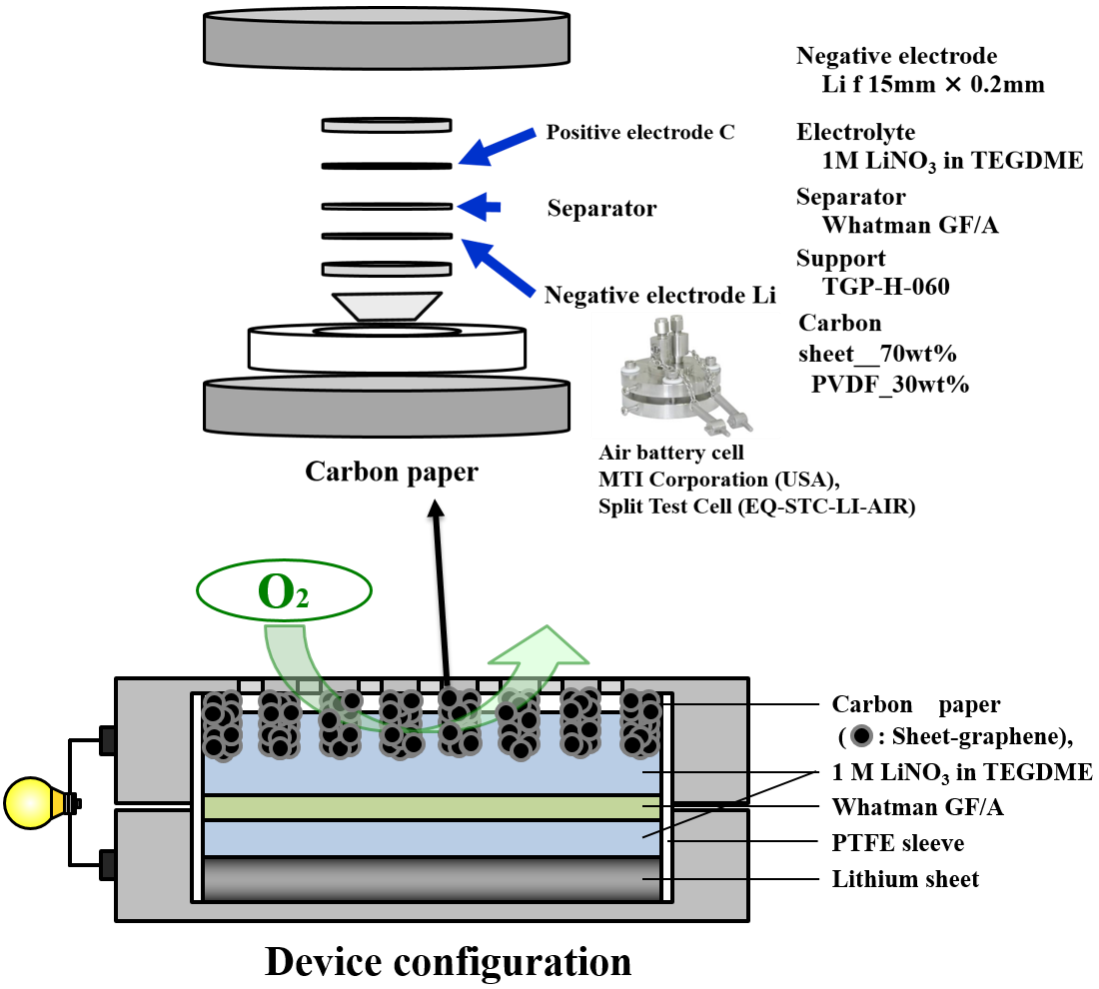

Fig. 4-2 The image of the fabricated Li-air Battery for nanocarbons.

4.2.4. *Fabrication of Li-air battery*

Li-air battery was fabricated in the Fig. 4-2. The air electrode was fabricated by mixture of nanocarbons and polyvinylidene difluoride (PVDF) and as binder in a weight ratio of 70:30 at 8 MPa. A lithium foil (thickness: 1 mm) was purchased (Honjo Chemical Corp., Japan). The air battery cells (MTI corporation, USA), and the electrode of 1M $LiNO_3$ in tetra ethylene glycol dimethyl ether (TEGDME) were used. Battery tests were conducted with a Solar Tron SI 1280 B at current density of 0.1 mA/cm^2 for discharge and 0.5 mA/cm^2 for charge. The cut off voltage in discharge was set to 2.0 V.

4.3. Results and discussion

4.3.1. *Synthesis rates*

Nanocarbons were synthesized using SPP from BZ, BZ-NO_2 and BZ-NH_2. After SSP, he synthesized nanocarbons were separated from liquid, dried and calculated the synthesis rates in Fig. 4-3. The highest carbon yield (Y) of BZ, BZ-NO_2 and BZ-NH_2 are 1.92, 0.32 and 0.48 %, respectively, at 150 KHz from the Table 4-S1.

The carbon yield (Y in %) and synthesis rate (R in mg/min) were calculated from the amount of carbon powders as:

$$Y = (M/M_0) \times 100$$

where M is the mass of the carbon powder, and M_0 is the initial mass of BZ, BZ-NO_2 and BZ-NH_2. However, the synthesis rate was calculate as $R = M/T$.

Where T is total process time (i.e., 30 min).

The nanocarbons are showed the lowest (42, 6 and 7 mg/min at 50 KHz, 0.5 μs) and highest (50, 13 and 15 mg/min at 150 KHz, 0.5 μs) synthesis rate for BZ, BZ-$NO_2$and BZ-NH_2 respectively. It confirm that, when the frequencies were gradually increased, the synthesis rate also increased with them. [43] In the case of BZ, the synthesis of nanocarbons were higher than BZ-NO_2 and BZ-NH_2 due to their structure. It means that only the π-conjugated bond is successfully enhanced the nanocarbon synthesis by SPP. Schematic of nanocarbon formation from BZ using SPP in the Fig. 4-S1. In this study, the highest synthesis rate of nanocarbons at 150 KHz, 0.5 μs are described for the future investigation. So far in the paper, we selected for the discussion only the data corresponding to the frequency of 150 KHz with the pulse width of 0.5 μs.

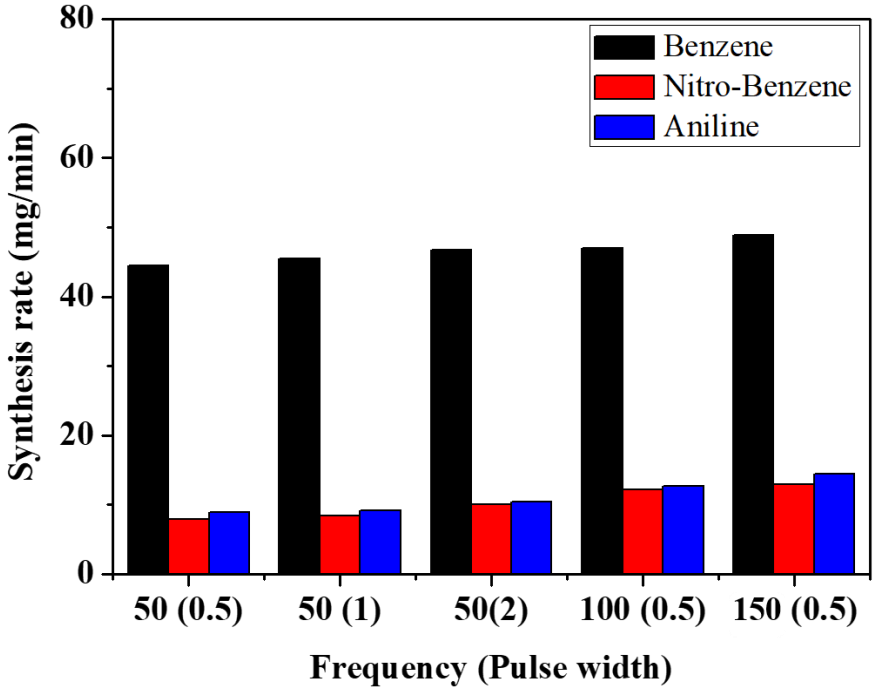

Fig. 4-3 The graph of the synthesis rate vs frequency (pulse width) of synthesized nanocarbons.

4.3.2. *Morphology and Surface area*

The TEM images were confirmed the morphology. The morphology of nanocarbons of BZ, BZ-$NO_2$and BZ-NH_2 by SPP were observed in Fig. 4-4 (a), (b) and (c). The average diameters were shows the 15-30 nm range of carbon with a ball-like shape. [44] The nanocarbons were agglomerated a few of the surface. The high-resolution TEM (HRTEM) images were showed in Fig. 4-4 (a′), (b′) and (c′). The graphite-like structure with a good crystallinity of nanocarbons were observed corresponding SAED images in Fig. 4-4 (a″), (b″) and (c″). The SAED images were showed the (002), (100), and (110) planes of nanocarbons. These date will confirm on XRD pattern.

To identify, the inside of the morphology such as surface area, pore size, and diameters were determined by Brunauer–Emmett–Teller (BET) in Table. 4-S2. BET surface area (220, 230 and 222 m^2g^{-1}), pore volume (0.45, 0.49 and 0.46 cm^3g^{-1}) and average pore diameter (20.0, 17.0 and

15.0 nm) were respectively BZ, BZ-NH_2 and BZ-NO_2 of nanocarbons. The nanocarbon of BZ-NH_2 was enhanced the surface area of 230 m^2 g^{-1}.

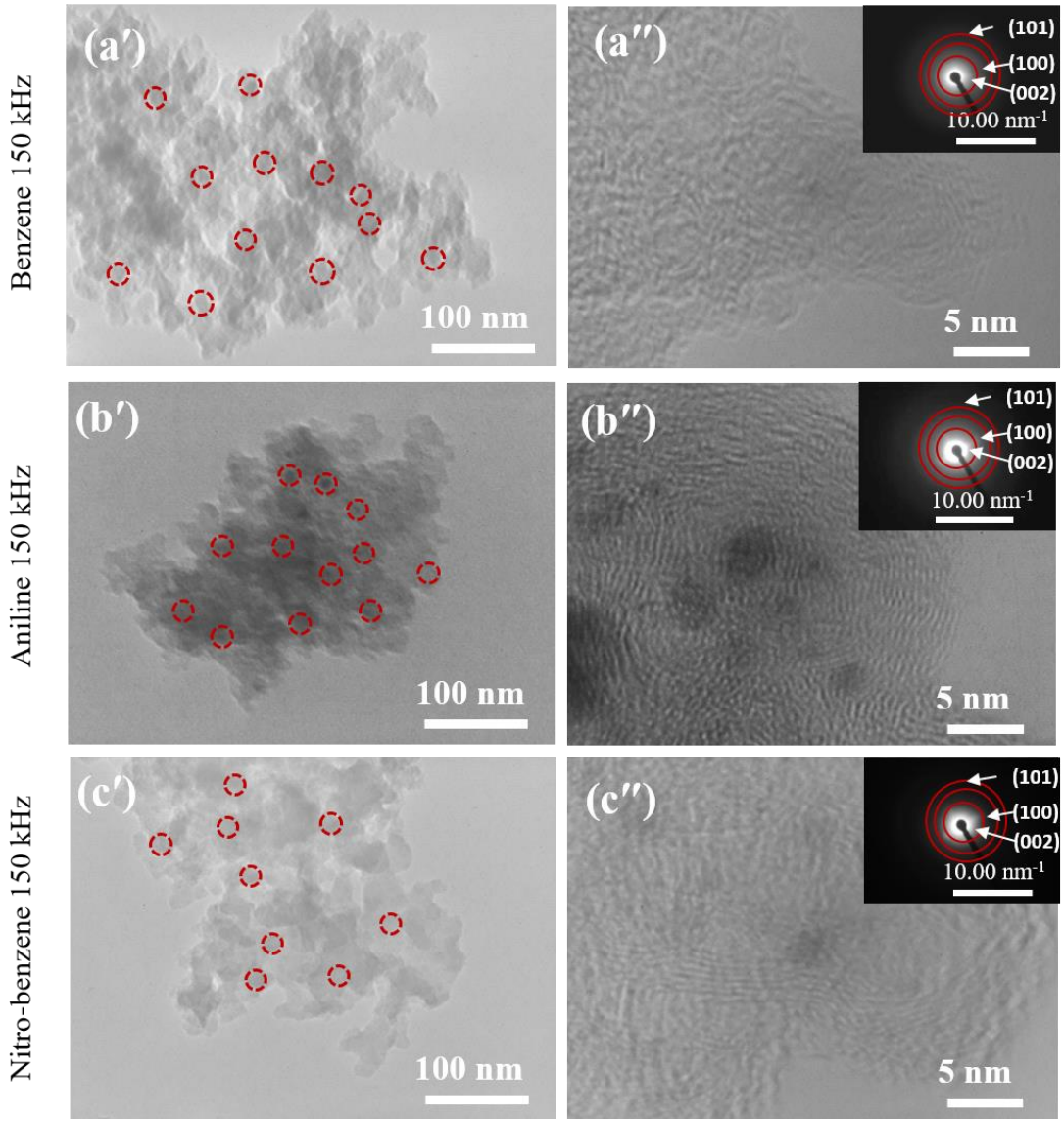

Fig. 4-4 TEM images of nanocarbons, (a), (b) and (c) TEM images; (a′), (b′) and (c′) HRTEM; and (a″), (b″) and (c″) SEAD pattern (insert) for BZ, BZ-NH2 and BZ-NO2 at 150 KHz and 0.5 μs.

4.3.3. *Structural properties*

The measurements of XRD patters and Raman spectra were showed in Fig. 4-5. The XRD peaks of BZ, BZ-NH_2 and BZ-NO_2 of nanocarbons were showed a large peak at 23° and a small

broadpeak at 44° respectively (002) and (100)/(101) planes of nanocarbon in Fig. 4-5 (a). [45, 46] The small and broad carbon shape were suggested that graphite plane (JCPDS 75-1621) with quite good crystallinity. The sharp peaks of tungsten carbide (WC) (JCPDS #25-1047) are obtained from the all samples at 36°, 42°, 62° and 74° correspond to the (111), (200), (220) (311) and (222) planes respectively. [47] In the case of BZ-NH_2 and BZ-NO_2 of nanocarbons, the WC peaks were increased due to a higher sputtering of tungsten electrode and the chemical structures compare with nanocarbon of BZ. The chemical structures of BZ (C-C, C=C and C-H), BZ-NO_2 (C-C, C=C, C-N, N=O and C-H) and BZ-NH_2 (C-C, C=C, C-N, N-H and C-H) are different. The sputtering rate is depend on the chemical structure of the solvents even the same plasma conditions. During the solution plasma process, solution conversion pathway is effect on the results.

Figure 4-5 (b) shows that the Raman peaks were observed D (1350 cm^{-1}) and G (1600 cm^{-1}) band of all samples. The D-band was showed the structural disorders and defects, [48] and G band was referred sp^2 graphite sheet-like structure nanocarbon. The I_D/I_G ratios of (0.80, 1.10 and 0.9) for the nanocarbons BZ, BZ-NH_2 and BZ-NO_2 were respectively calculated from the peaks. The I_D/I_G values were indicated defect sites with degree of graphitization for nanocarbons. [49]

The I_G/I_D ratio was related to the crystallite size L_a and Tuinstra–Koenig relationship as follows.

L_a (nm) = $(2.4 \times 10^{-10}) \lambda^4 (I_G/I_D)$, [50]

where λ is the Raman excitation wavelength at 532 nm. The L_a values were consisted the inter-defect distance of the surface. The L_a values of nanocarbon of BZ-NH_2 was showed a more defect sites due to their nitrogen molecules.

The XRD and Raman results were corresponded with the TEM images that the nanocarbons were graphite like structure with a crystallinity.

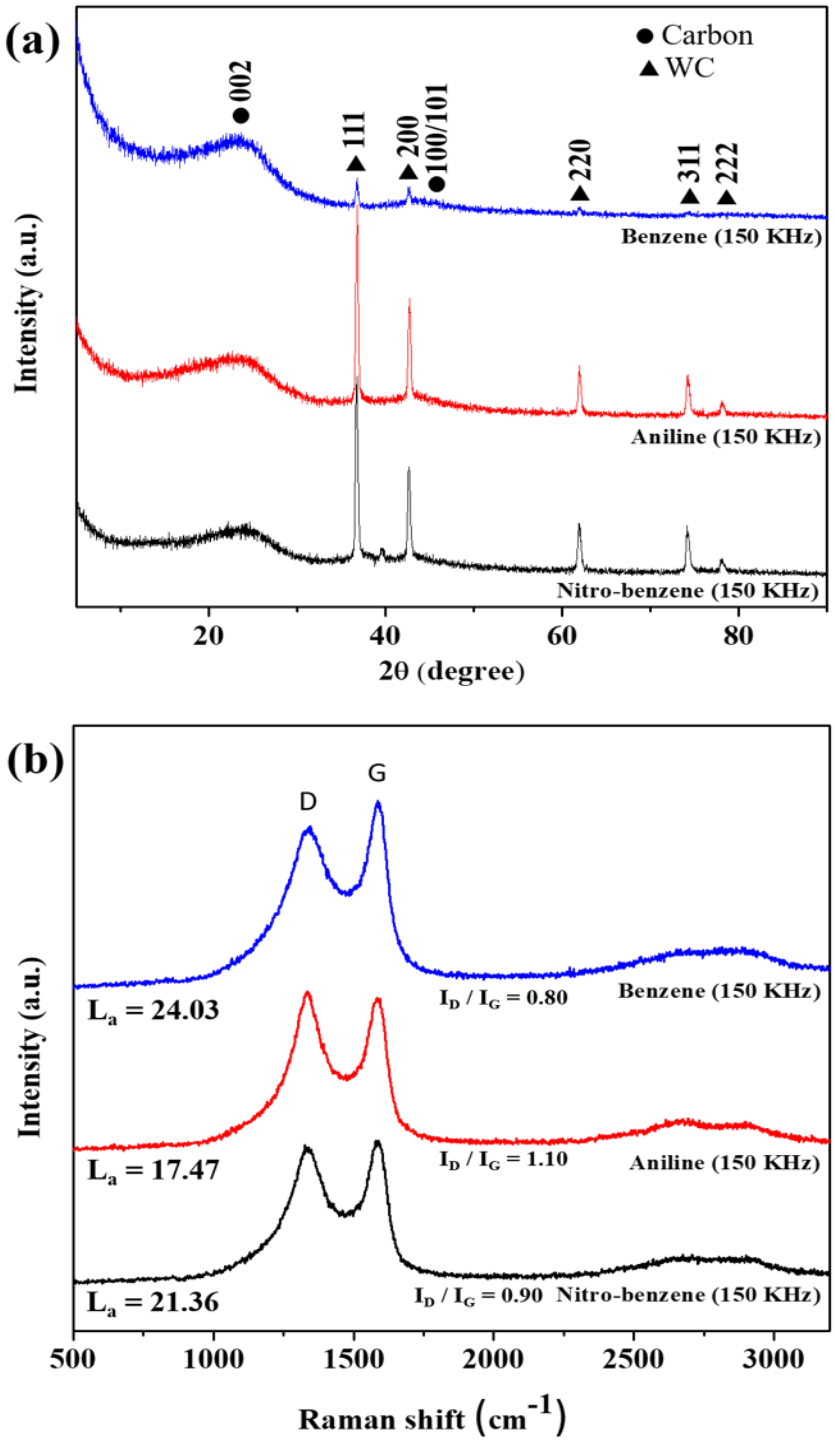

Fig. 4-5 The structural properties of nanocarbon a) XRD patters, and b) Raman spectra for nanocarbons of BZ, BZ-NH2 and BZ-NO2 at 150 KHz and 0.5 μs.

4.3.4. *Electrical conductivity and compositions*

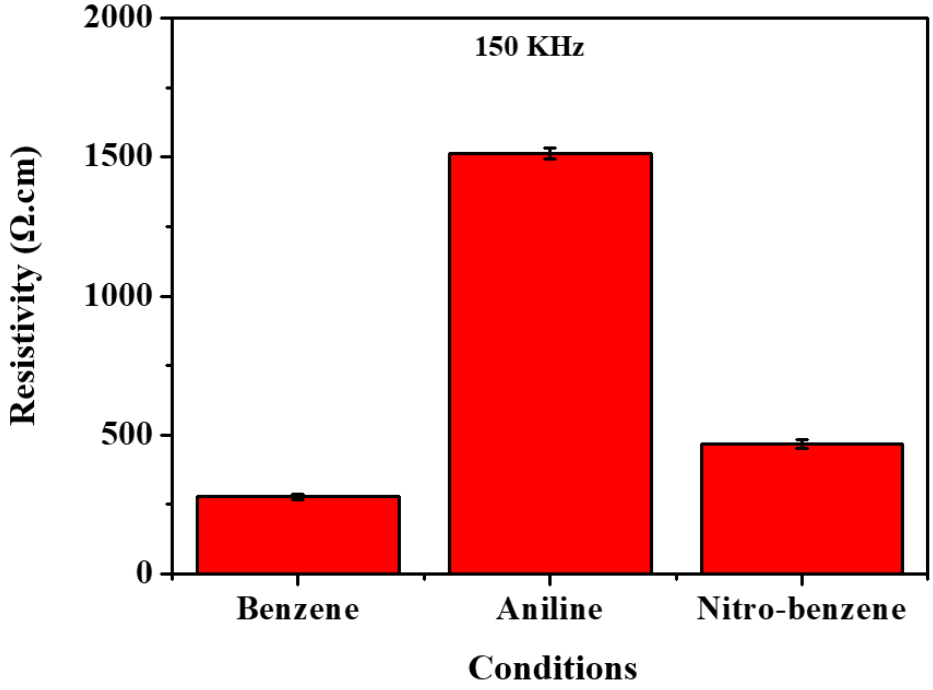

Fig. 4-6 Image of electrical resistivity by four probe for nanocarbons at various conditions.

The four-point probe method was applied on nanocarbon to identify Resistance (Ω), Surface resistance (Ω/cm^2), Resistivity (Ω.cm) and Electrical conductivity (s/cm) in Table 4-S3, Table 4-S4 and Table 4-S5 corresponding in Fig. 4-6. So, we observed that when the resistivity (Ω.cm) of nanocarbon was decreased, the conductivity was increased. In the case of nanocarbon of BZ, it's showed the highest electrical conductivity compare with the nanocarbon of BZ-NH_2 and BZ-NO_2. The surface elemental composition was founded by XPS spectroscopy shown in Fig. 4-S2. The nanocarbons of BZ (C1s 99.6, and W4f 0.4 atom %), nanocarbon of BZ-NH_2 (C1s 98.2, N1s 1.6, and W4f 0.2 atom %), and nanocarbon of BZ-NO_2 (C1s 97.1, O1s 15.9, N1s 5.0 and W <0.1, atom %) were identified at 150 KHz and 0.5 µs. From the XPS spectroscopy of nanocarbons data were showed that nanocarbons of BZ containing carbon (C) and tungsten (W); nanocarbons of BZ-NH_2 containing carbon (C), nitrogen (N) and tungsten (W); and nanocarbon of BZ-NO_2 containing carbon (C), Oxygen (O), nitrogen (N) and tungsten (W)

corresponding with XRD patterns.

4.3.5. *Catalytic activity*

The electrocatalytic activity of ORR were also tested in 0.5 mol/L H_2SO_4 solution with N_2 and O_2 saturated at 20 mV s^{-1} scan rate in Fig. 4-7 (a), (b) and (c). The anodic and cathodic peaks were showed the potential range at –0.2 to 1.2 V. In the N_2-saturated of nanocarbons BZ and BZ-NO_2 were observed the featureless CV curve in Fig. 4-7 (a) and Fig. 7 (b).Oh the other hand, the CV curve under O_2-saturated electrolyte was observed the cathodic peak around at 0.4 V corresponding to ORR. The catalytic activity of ORR concerns in fuel-cell applications as a cathode.

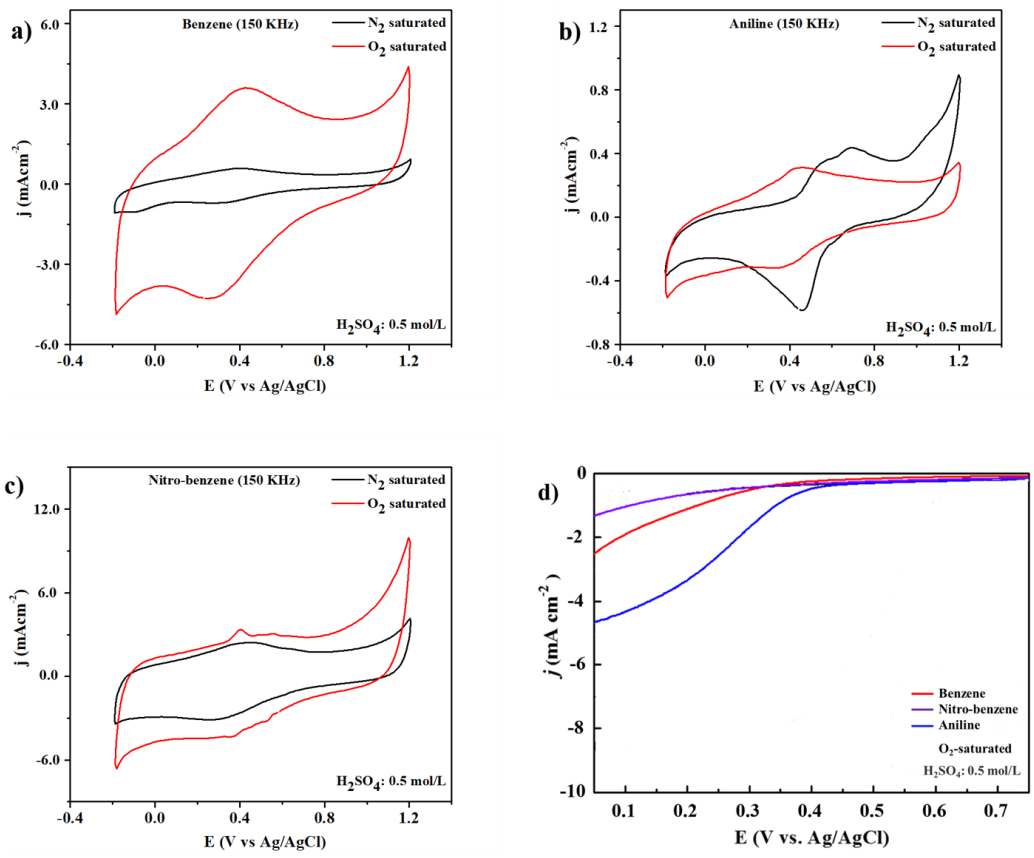

Fig. 4-7 CV measurements CV measurements of (a) benzene (BZ), b) aniline (BZ-NH_2) and c) nitrobenzene (BZ-NO_2) in 0.5 mol/L H_2SO_4 solution at a scan rate of 20 mV s^{-1} under N_2 (black

line) and O_2 (red line) saturated. LSV measurements of d) presents the LSV curves of BZ, BZ-NH_2, and BZ-NO_2 an O_2-saturated 0.5 mol/L H_2SO_4 solution at a scan rate of 10 mV s^{-1} with a rotation speed of 1600 rpm.

Fig. 7d) presents the LSV curves of BZ, BZ-NO_2 and BZ-NH_2 an O_2-saturated 0.5 mol/L H_2SO_4 solution at a scan rate of 10 mV s^{-1} with a rotation speed of 1600 rpm. The LSV curve was obtained an onset potential of 0.39 V of BZ-NH_2. Moreover, the current density of BZ-NH_2 also larger than BZ and BZ-NO_2 were investigated. Nanocarbon of BZ-NH_2 showed the synergistic effect of N and WC containing on the ORR activity. The specific capacity shows such a difference with various nanocarbons due to their properties of tungsten (W), nitrogen (N) and Oxygen (O) containing nanocarbons. In the case of BZ-NH_2, the synergistic effect of N and WC doping on the ORR activity compare with the BZ and BZ-NO_2. BZ-NH_2 showed the enhanced carbon properties, such as surface area, resistivity, nitrogen configuration and degree of graphitization played a role in the improved ORR activity in the acid media compared with BZ and BZ-NO_2.

4.3.6. *Li-air battery test*

The electrochemical performances of the cell voltage and capacity of Li-air batteries, the discharge of 1.0 mg/cm^2 carbon loading in 1.0 atom of dry oxygen at 0.1 mA/cm^2 rates are shown in Fig. 4-8. The specific capacity of 2800, 3600, 6700 and 15000 mAh/g carbon were identified from nanocarbons of BZ-NO_2, palm oils, BZ and BZ-NH_2 respectively at the rate of 0.1 mA/cm^2 with the 1.0 mg/cm^2 carbon loading. The highest special capacity of 15500 mAh/g carbon has been obtained for nanocarbon of BZ-NH_2 compare with nanocarbon of palm oils.

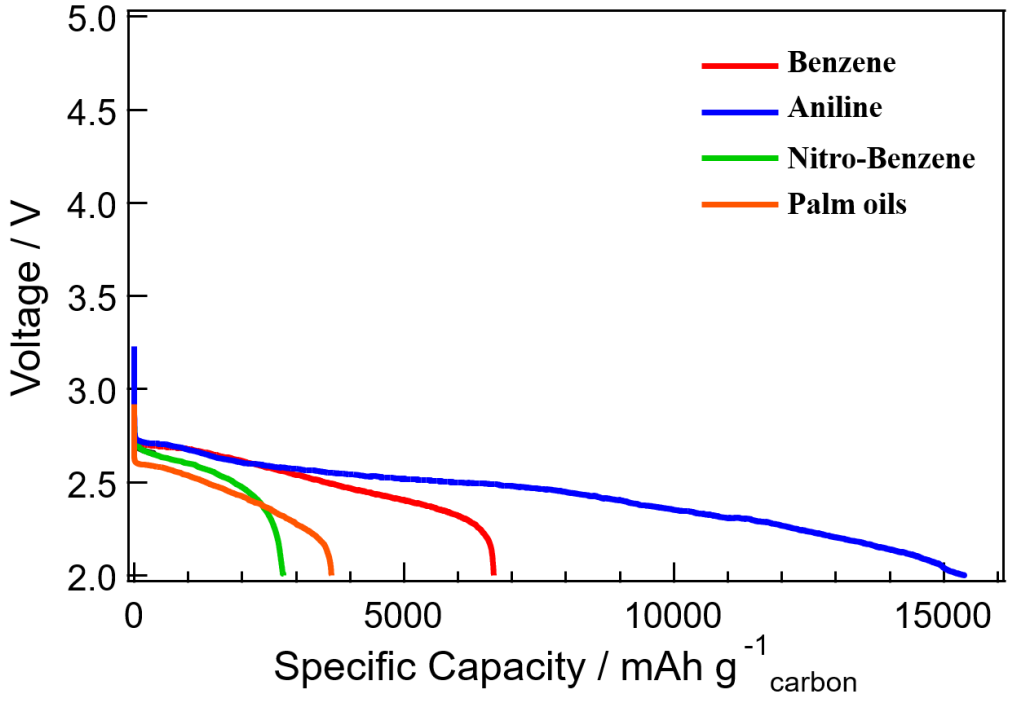

Fig. 4-8 The discharge curves of the Li-air batteries with the 1.0 mg carbon loadings at 0.1 mA/cm2rates for nanocarbons of BZ, BZ-NH2, BZ-NO2, palm oils.

4.4. Summary

We have been synthesized the nanocarbons by solution plasma process. The highest synthesis rate was observed form the nanocarbon of BZ. The graphite-like structure and the range of 15-30 nm sized of nanocarbons were investigated from the TEM image supported with XRD and Raman spectroscopy measurements. For the electrocatalytic activity of ORR of nanocarbons were clearly observed the cathodic peak at 0.4 V for all samples. The performance of Li-air battery, the highest special capacity of 15500 mAh/g carbon from nanocarbons of BZ-NH_2 was compared with nanocarbon of palm oils. We believe that SPP could be able to synthesis the nanocarbons and their applications of electrocatalitic activity such as Li-air batteries and fuel cell.

References

1) S. W. Lee, N. Yabuuchi, B. M. Gallant, S. Chen, B.-S. Kim, P. T. Hammond and Y. Shao-Horn, Nat. Nanotechnol., 5, 531 (2010).
2) A. Chen and P. Holt-Hindle, Chem. Rev., 110, 3767 (2010).
3) X. Ma, H. Meng, M. Cai and P. Shen, J. Am. Chem. Soc., 134, 1954 (2012).
4) Y. Zhao, L. Yang, S. Chen, X. Wang, Y. Ma, Q. Wu, Y. Jiang, W. Qian and Z. Hu, J. Am. Chem. Soc., 135, 1201 (2013).
5) B. Winther-Jensen, O. Winther-Jensen, M. Forsyth and D. R. MacFarlane, Science, 321, 671 (2008).
6) Y. Zheng, Y. Jiao, J. Chen, J. Liu, J. Liang, A. Du, W. Zhang, Z. Zhu, S. C. Smith, M. Jaroniec, G. Q. Lu and S. Z. Qiao, J. Am. Chem. Soc., 133, 20116 (2011).
7) Z. Schnepp, Y. Zhang, M. J. Hollamby, B. R. Pauw, M. Tanaka, Y. Matsushita and Y. Sakka, J. Mater. Chem. A, 1, 13576 (2013).
8) H. Wang, T. Maiyalagan and X. Wang, ACS Catal., 2, 781 (2012).
9) C. Soldano, A. Mahmood and E. Dujardin, Carbon, 48, 2127-2150 (2010).
10) A. Manikandan, L. Lee, Y.-C. Wang, C.-W. Chen, Y.-Z. Chen, H. Medina, J.-Y. Tseng, Z. M. Wang and Y.-L. Chueh, J. Mater. Chem. A, 5, 13320-13328 (2017).
11) Z. Yang, W. Sun, L. Wang, Z. Wan, J. Wang, S. Wang and G. Liu, Corros. Sci., 175, 108860 (2020).
12) M. Topsakal, H. Şahin and S. Ciraci, Phys. Rev. B, 85, 155445 (2012).
13) J. Liang, Y. Jiao, M. Jaroniec and S. Z. Qiao, Angew. Chem. Int. Ed., 51, 11496-11500 (2012).
14) Q. Lv, W. Si, J. He, L. Sun, C. Zhang, N. Wang, Z. Yang, X. Li, X. Wang and W. Deng, Nat. Commun., 9, 1-11 (2018).
15) S. Chen, A. Zehri, Q. Wang, G. Yuan, X. Liu, N. Wang and J. Liu, ChemistryOpen, 8, 58-63 (2019).

16) W. Lei, H. M. Barnes, J. Zhang and Z. Cai, Wood Fiber Sci., 49, 22-32 (2017).

17) S. W. Lee, B. M. Gallant, H. R. Byon, P. T. Hammond and Y. Shao-Horn, Energy Environ. Sci., 4, 1972 (2011).

18) S. W. Lee, B.-S. Kim, S. Chen, Y. Shao-Horn and P. T. Hammond, J. Am. Chem. Soc., 131, 671 (2009).

19) A. Watthanaphanit, G. Panomsuwanc and N. Saito, RSC Adv., 4, 1622 (2014).

20) G. Panomsuwan, A. Watthanaphanit, T. Ishizaki and N. Saito, Phys. Chem. Chem. Phys., 17, 13794 (2015).

21) T. Ishizaki, S. Chiba, Y. Kaneko and G. Panomsuwan, J. Mater. Chem. A, 2, 10589-10598 (2014).

22) T. Morishita, T. Ueno, G. Panomsuwan, J. Hieda, A. Yoshida, M. A. Bratescu and N. Saito, Sci. Rep., 6, 36880 (2016).

23) X. Hu, X. Shen, O. Takai and N. Saito, J. Alloys Compd., 552, 351-355 (2013).

24) S. Chae, G. Panomsuwan, M. A. Bratescu, K. Teshima and N. Saito, ACS Appl. Nano Mater., 2, 1350-1355 (2019).

25) C. Chokradjaroen, S. Kato, K. Fujiwara, H. Watanabe, T. Ishii and T. Ishizaki, Sustain. Energy Fuels, 4, 4570–4580 (2020).

26) O. L. Li, S. Chiba, Y. Wada, G. Panomsuwan and T. Ishizaki, J. Mater. Chem. A, 5, 2073-2082 (2017).

27) M. A. Bratescu, O. Takai and N. Saito, J. Alloys Compd., 562, 74-83 (2013).

28) K. Hyun, T. Ueno, O. L. Li and N. Saito, RSC Adv., 6, 6990- 6996 (2016).

29) C. H. Choi, S. H. Park and S. I. Woo, J. Mater. Chem., 22, 12107-12115 (2012).

30) G. Panomsuwan, N. Saito and T. Ishizaki, J. Mater. Chem. A, 3, 9972-9981 (2015).

31) N. Thongwichit, O. L. H. Li, W. Yaowarat, N. Saito and U. Suriyapraphadilok, Jpn. J. Appl. Phys., 55, 01AE10 (2015) .

32) J. Kim, J. Chun, S.-G. Kim, H. Ahn and K. C. Roh, J. Electrochem. Sci. Technol, 8, 338-343 (2017).

33) D.-w. Kim, O. L. Li and N. Saito, Phys. Chem. Chem. Phys., 16, 14905-14911 (2014).

34) O. Takai, Pure Appl. Chem., 80, 2003–2011 (2008).

35) G. Panomsuwan, N. Saito and T. Ishizaki, Phys. Chem. Chem. Phys., 17, 6227 (2015).

36) W. Wang, S. Chakrabarti, Z. Chen, Z. Yan, M. O. Tade, J. Zou and Q. Li, J. Mater. Chem. A, 2, 2390-2396 (2014).

37) T. Sudare, T. Ueno, A. Watthanaphanit and N. Saito, Phys. Chem. Chem. Phys., 17, 30255-30259 (2015).

38) K. Hyun, T. Ueno, O. L. Li and N. Saito, RSC Adv., 6, 6990-6996 (2016).

39) T. Morishita, T. Ueno, G. Panomsuwan, J. Hieda, A. Yoshida, M. A. Bratescu and N. Saito, Scientific Reports, 6, 36880 (2016).

40) J. Kang, O. L. Li and N. Saito, Nanoscale, 5, 6874 (2013).

41) D. Kim, O. L. Li, P. Pootawang and N. Saito, RSC Adv., 4, 16813 (2014).

42) S. Lee, Y. Heo, M. A. Bratescu, T. Ueno and N. Saito, Phys. Chem. Chem. Phys., 00, 1-11 (2017).

43) O. L. Li, H. Hayashi, T. Ishizaki and N. Saito, RSC Adv., 6, 51864 (2016).

44) D. Kim, O. L. Li and N. Saito, Phys. Chem. Chem. Phys., 17, 407 (2015).

45) G. Panomsuwan, S. Chiba, Y. Kaneko, N. Saito and T. Ishizaki, J. Mater. Chem. A, 2, 18677 (2014).

46) X. Zhang and Z. Lix, Nanoscale, 4, 707-714 (2012).

47) T. Murphy, R. Hayes, S. Imberti, G. G. Warr and R. Atkin, Phys. Chem. Chem. Phys., 16, 13182-13190 (2014).

48) K. F. Adekunle, J. Poly. Chem., 5, 34-40 (2015).

49) N. Taufiqurrahmi and S. Bhatia, Energy Environ. Sci., 4, 1087-1112 (2011).

50) L. G. Cançado, K. Takai, T. EnokiM. Endo, Y. A. Kim, H. Mizusaki, A. Jorio, L. N. Coelho, R. M. Paniago, and M. A. Pimenta, Appl. Phys. Lett., 88, 163106 (2006).

Supplementary information

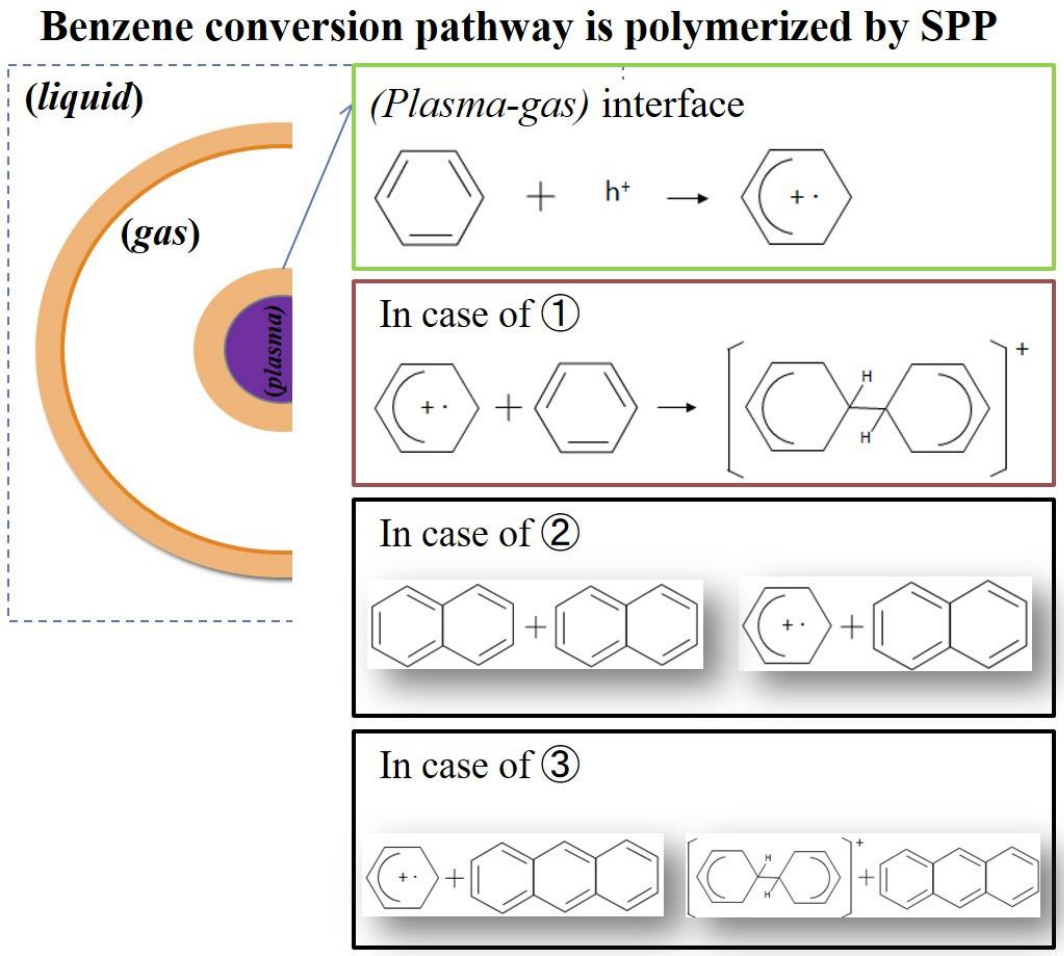

Fig. 4-S1 Schematic of nanocarbon formation from BZ using SPP.

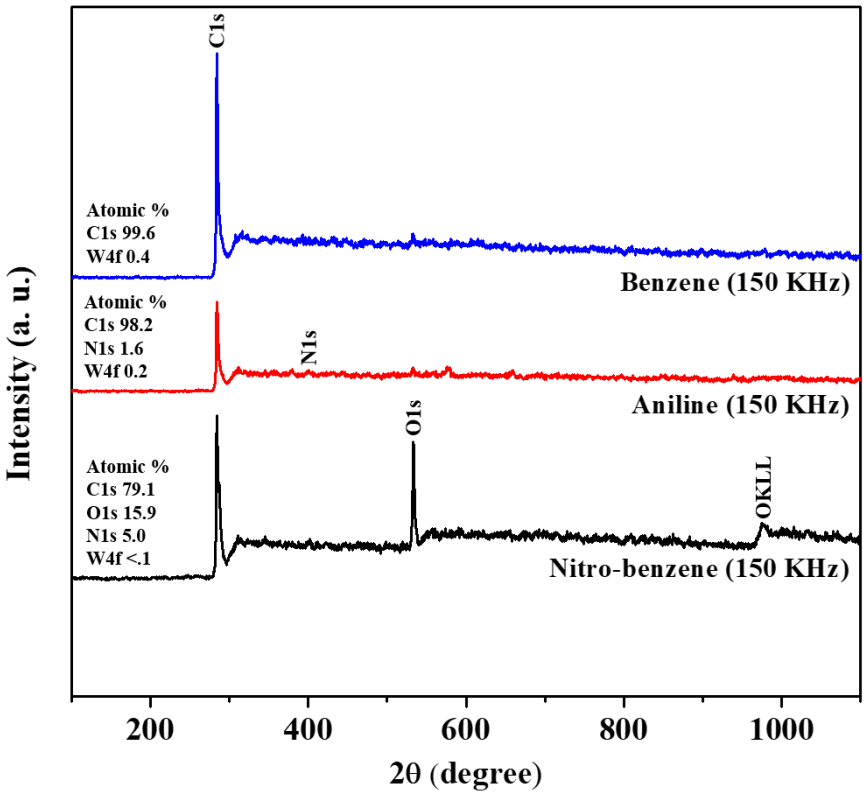

Fig. 4-S2 XPS elemental compositions (% atom) of nanocarbons of BZ, BZ-NH_2 and BZ-NO_2.

Table S1. The carbon yield (%) and synthesis rate are calculated form the carbon powder

Conditions	Carbon Powder, M (mg)	Synthesis rate, R (mg/min)	Carbon yield, Y (%)
BZ (50 KHz, 0.5 µs)	1260	42	1.61
BZ (150 KHz, 0.5 µs)	1500	50	1.92
BZ-NO_2 (50 KHz, 0.5 µs)	180	6	0.15
BZ-NO_2 (150 KHz, 0.5 µs)	390	13	0.32
BZ-NH_2 (50 KHz, 0.5 µs)	210	7	0.23
BZ-NH_2 (50 KHz, 0.5 µs)	450	15	0.48

Table 4-S2 SPP conditions for the conversion of palm oil to nanocarbon composite for 1 μs and 40 min discharge.

Frequency (kHz)	Surface area (m^2/g)	Pore volume (cm^3/g)	Average pore diameter (nm)
BZ	220	0.45	20.0
BZ-NH_2	230	0.49	17.0
BZ-NO_2	222	0.46	15.0

Table 4-S3 The resistance (Ω), surface resistance (Ω/cm2), resistivity (Ω.cm) and electrical conductivity (s/cm) tested by four-point probe in the different conditions for benzene.

Conditions	Film thickness (μm)	Resistance (Ω)	Surface restance (Ω/cm^2)	Electrical conductivity (s/cm)	Resistivity (Ω.cm)
Benzene (150 kHz,0.5 μs)	88	$6.98x10^3$	$3.16x10^4$	$3.59x10^{-3}$	278.4
Benzene (100 kHz,0.5 μs)	112	$7.89x10^3$	$3.57x10^4$	$2.53x10^{-3}$	395.9
Benzene (50 kHz,0.5 μs)	95	$9.88x10^3$	$4.48x10^4$	$2.48x10^{-3}$	403.0

Table 4-S4. The resistance (Ω), surface resistance (Ω/cm2), resistivity (Ω.cm) and electrical conductivity (s/cm) tested by four-point probe in the different conditions for Aniline.

Conditions	Film thickness (μm)	Resistance (Ω)	Surface restance (Ω/cm^2)	Electrical conductivity (s/cm)	Resistivity (Ω.cm)
Aniline (150 kHz,0.5 μs)	70	$5.29x10^4$	$2.40x10^5$	$6.61x10^{-4}$	1513
Aniline (100 kHz,0.5 μs)	76	$6.06x10^4$	$2.75x10^5$	$5.78x10^{-4}$	1729
Aniline (50 kHz,0.5 μs)	63	$8.31x10^4$	$3.77x10^5$	$4.22x10^{-4}$	2373

Table 4-S5. The resistance (Ω), surface resistance (Ω/cm2), resistivity (Ω.cm) and electrical conductivity (s/cm) tested by four-point probe in the different conditions for Nitro-benzene.

Conditions	Film thickness (μm)	Resistance (Ω)	Surface restance (Ω/cm^2)	Electrical conductivity (s/cm)	Resistivity (Ω.cm)
Nitro-Benzene(150 kHz,0.5 μs)	181	$9.30x10^3$	$4.22x10^4$	$2.14x10^{-3}$	467.8
Nitro-Benzene (100 kHz,0.5 μs)	170	$7.05x10^3$	$3.19x10^4$	$1.72x10^{-3}$	577.4
Nitro-Benzene (50 kHz,0.5 μs)	164	$7.70x10^3$	$3.17x10^4$	$1.73x10^{-3}$	581.4

Chapter 5

Solid state bio fuel cell fabricated by carbon nanohorns for biomedical applications

Chapter 5 – Solid state bio fuel cell fabricated by carbon nanohorns for biomedical applications

5.1. Introduction

CMOS-compatible products offer high-performance in terms of low-power computing, sensing, and communications to IoT-based healthcare systems. To satisfy these demands, several CMOS biosensor LSIs have been developed. [1–3] CMOS technology can also improve the energy efficiency of IoT-based healthcare systems. However, energy-autonomous operations that use energy harvesting techniques have proved to be difficult to establish.

The main components in the design of glucose fuel cells are CNHs. [4] 1D structural single-walled CNHs are a newly-developed carbon material. [5] They are similar to single-walled carbon nano tubes (SWCNTs). [6–8] CNHs have possible future applications across a wide range of materials fields. D-Glucose fuel cells are valuable power sources in biomedical areas, and for human homeostasis. [9–11] These fuel cells are mainly generated by the electrochemical reaction between glucose and oxygen that occurs at electrodes. Glucose and oxygen are available in bodily fluids, such as blood, and interstitial fluid allows for the continuous production of electricity. These are the main advantages of the human body. The advantages of using CNHs as catalysts include

that they exhibit less specificity and lower reaction rates compared with SWCNTs.

In recent years, glucose fuel cells have increasingly been used in solid-state CMOS bioelectronics devices, due to rapid improvements in their energy efficiency and function. [12–21] Solid-state CMOS-compatible glucose fuel cells were developed for integration with CMOS circuitries and small systems. [22]

However, these small systems showed low invasiveness in the limited power generation capacity of their fuel cells, which is required for their circuitries to be energy efficient. In spite of these advantages, their applications are limited because of their low output power. [23–25] The energy sources for emerging next-generation internet of things (IoT)-based healthcare systems have since been applied. In 2012, a CMOS-compatible glucose sensor was proposed and developed. [26]

This work presents a proposal and for a new structure for improving the OCV. The performance of the fuel cell was enhanced by improving the electrocatalytic ability of the anode. An OCV of 375 mV was achieved, which is the highest value ever reported. This achievement will contribute to the developments of next-generation IoT-based healthcare technology for biomedical applications.

5.2. Experimental procedure

5.2.1 *Measurement Methods*

The systematic illustration of the CMOS-compatible glucose fuel cell are shown in Fig. 5-1. However, Raney platinum, which is used as a reagent, is a porous platinum. [25, 27] The main chemical reactions of Raney platinum are as follows:

Anode: $C_6H_{12}O_6 + H_2O \rightarrow C_6H_{12}O_7 + 2H^+ + 2e^-$,

Cathode: $1/2O_2 + 2H^+ + 2e^- \rightarrow H_2O$,

Whole: $C_6H_{12}O_6 + 1/2O_2 \rightarrow C_6H_{12}O_7$.

As shown above, the oxidation of glucose and the reduction of oxygen occur at the anode and the cathode, respectively. The theoretical electromotive force generated due to the partial reaction is 1.30 V. [28, 29]

The fabrication process of the CMOS-compatible glucose fuel cell is shown in Fig. 5-2. Firstly, a 6-in silicon wafer, with a 1 μm thermal oxide, was prepared with a wafer thickness of 625 μm. The fabricated area was 17.5 mm × 0.7 mm for each side and the anode surface area was 16.2 mm × 0.3 mm. The cathode surface morphology was too rough after fabrication using CNHs, however. Secondly, the footprint and anode area were patterned with a wet process. Titanium and platinum of 2 nm and 100 nm thickness, respectively, were deposited. Titanium was used as an adhesive layer. Thirdly, a 100-nm-thick aluminium layer was deposited on the platinum in the anode area. This was annealed, and a Pt/Al alloy was formed in the anode area. After annealing, the Al was etched from the Pt/Al alloy, so that only the porous Pt remained.

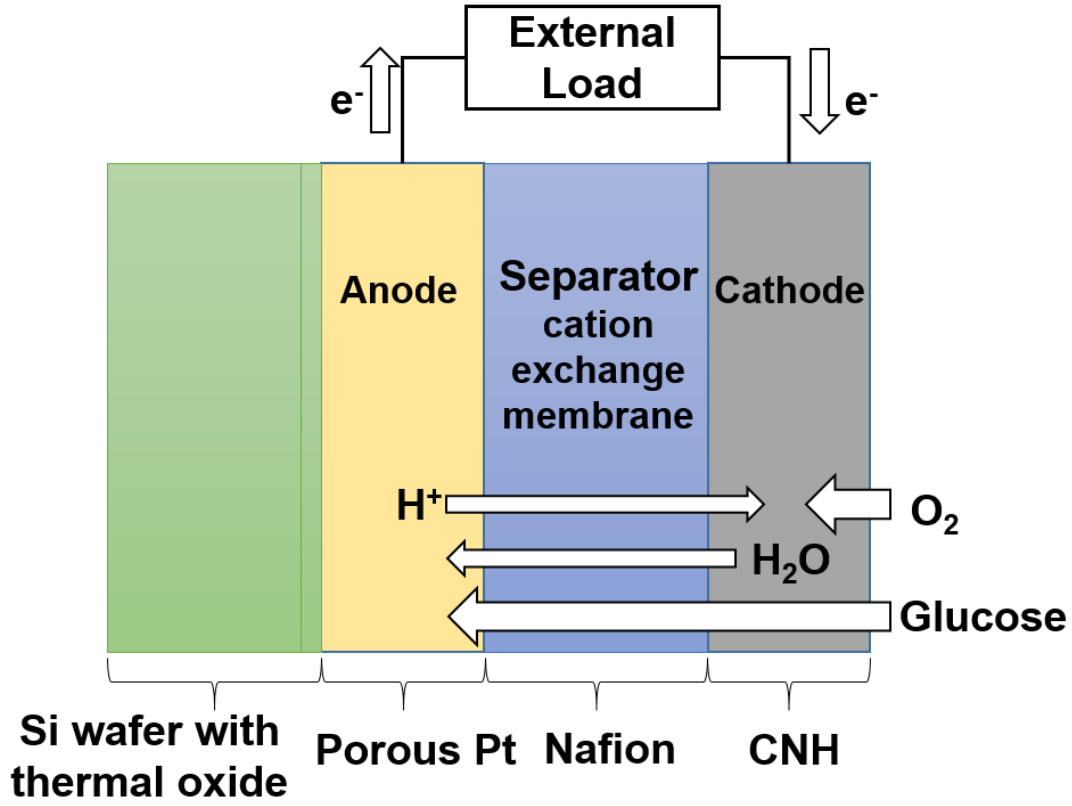

Fig. 5-1 Systematic illustration of the CMOS-compatible glucose fuel cell.

The anode area occupied 16.2 mm × 0.3 mm. The ratio of Pt/Al was 1:1, due to their 100 nm layers on the wafer. Fourth, Nafion solution was prepared via a 1:5 dilution in 2-propanol (IPA) from Nafion liquid dispersion [Nafion® perfluorinated resin solution (5 wt. %) in a mixture of lower aliphatic alcohols and water, containing 45% water (Sigma-Aldrich)]. The Nafion solution was spin-coated at 400 rpm then heated at 60 °C and 120 °C, for 30 min at each temperature. This coating and heating process was repeated to form a thick Nafion layer. After the second coating and heating procedure, the formed Nafion layer was patterned using photolithography. Finally, single-walled CNHs (1-7 wt.%) were dispersed in 0.83 % Nafion solution with ethanol (C_2H_5OH) to form a CNHs dispersed solution. CNHs from the NEC Corporation Japan were used.

The CNHs solution was spin-coated once, before being heated at 80 °C for three hours in an oven. The CNHs-based layer was then patterned onto the wafer as Fig. 5-S1.

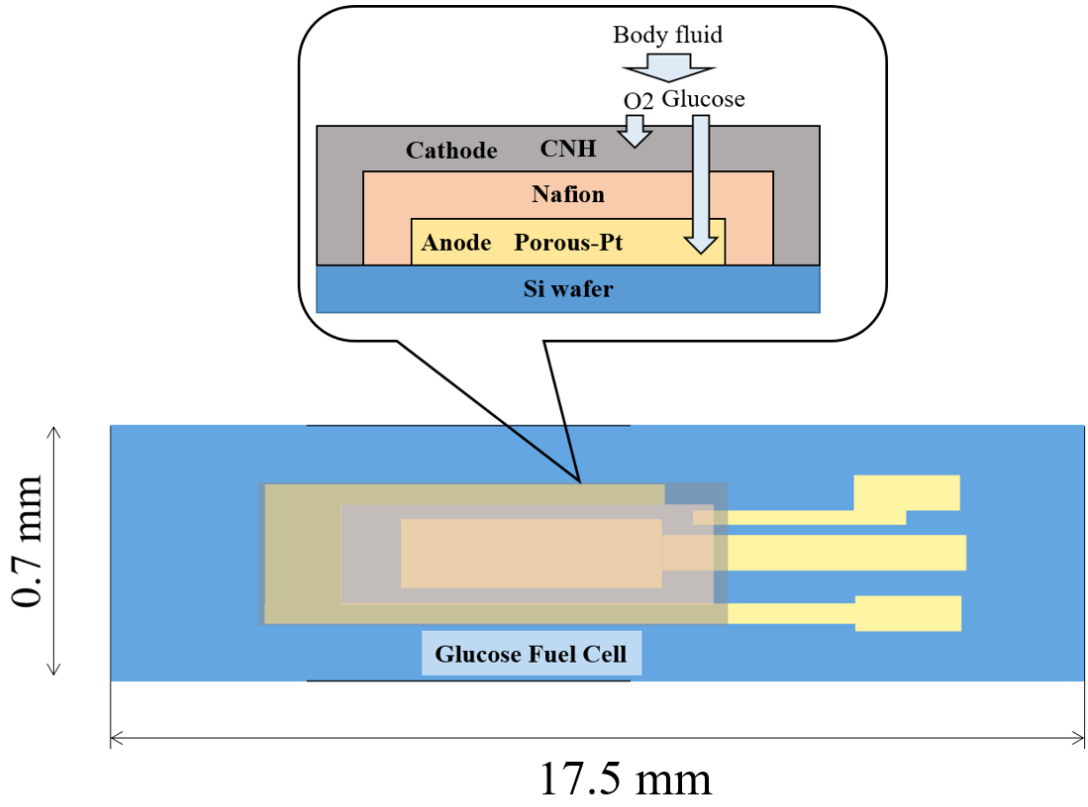

Fig. 5-2 Systemic image of the development procedure.

5.2.2 *Measurement setup*

Firstly, the manual prober and a DC multi-contact probe were used to establish electrical contact with the developed cells. Electrical measurements were verified with a tester (U1225A, Agilent Technologies) and a source measure unit (SMU; GS610, Yokogawa). The measurements were performed after dropping a phosphate-buffered saline (PBS)-based glucose solution onto the cathode area. The load depends on the SMU; in the case of this study, both the supply current and the measured voltage, or the supply voltage and current, were observed. The glucose solution was prepared with D (+)-Glucose (Wako) and PBS 10X (Irvine Scientific). 30 mM glucose solution was used in these experiments.

5.3. Results and discussion

5.3.1. *Results*

Figure 5-3 shows the voltage and current dependence on the power of the CNHs (1, 3, 5, and 7 % respectively) regarding the measurement of the OCV in 30 mM glucose solution. The CNHs (1, 3, 5, and 7 wt.%), voltage (355, 375, 310, and 291 mV), current (1.10, 1.12, 1.06, and 1.01 μA), and power density (8.02, 8.64, 6.76, and 6.17 μW/cm2) are shown. For the 3 wt.% CNHs, the highest OCV that was obtained is 375 mV, and the peak power density is 8.64 $\mu W/mm^2$ when the current density is 23.05 $\mu A/cm^2$. It is assumed that this output is an important for the fuel cell performance. Figure 5-S2 shows the CMOS-compatible glucose fuel cell images for (a) CNHs 1 wt.%, (b) CNHs 3 wt.%, (d) CNHs 5 wt.%, and (d) CNHs 7 wt.%. The power density, compared with CNHs wt.%. is shown in Figure 5-S3.

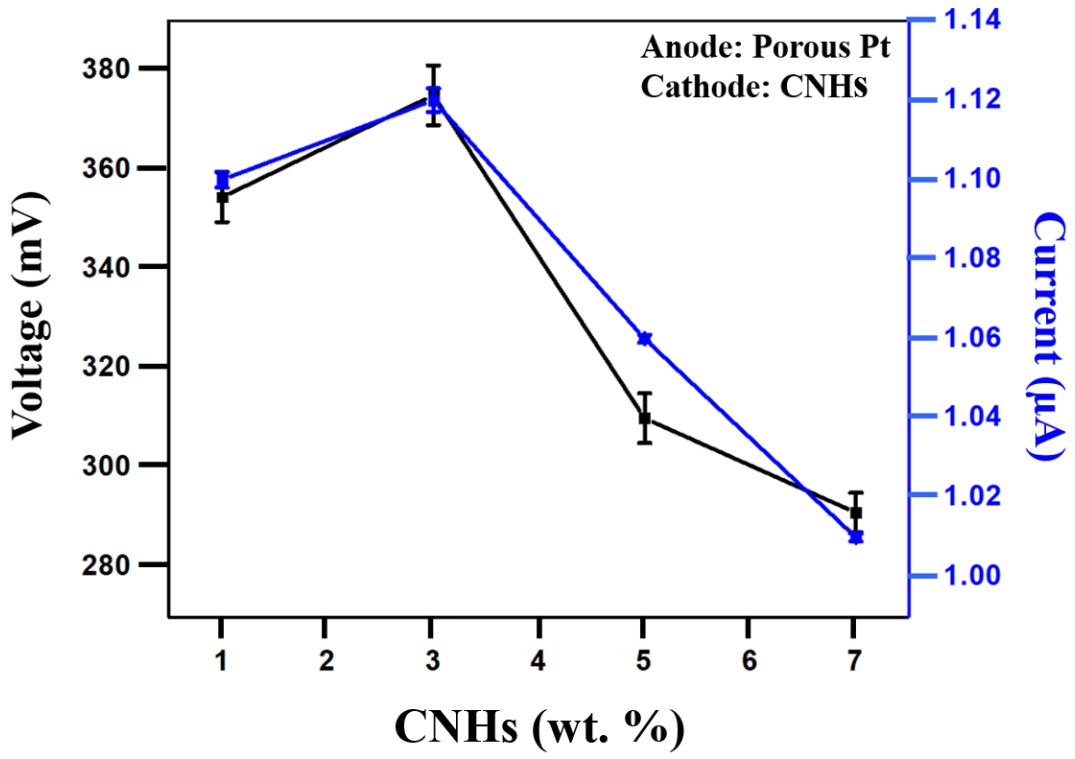

Fig. 5-3 Measured CNHs wt.% dependent on the current and voltage results.

5.3.2. *Discussion*

Figure 5-S3 shows that the results of the 3 wt.% CNHs on wafer-scale CMOS compatible glucose fuel cells achieved the highest OCV value. Various amounts (wt.%) of CNHs can be used to develop CMOS-compatible fuel cells with different OCVs and electrical conductivities for biomedical applications. The fuel cell was diffused on the anode surface. The anode reaction rate depends on the fuel concentration on its surface, meaning that current density is affected by the amount of CNHs (wt.%) due to their less specificity and lower reaction rates. [30, 31] When the CNHs wt.% is increased, the voltage and current decreased from 3 wt.%. After the glucose fuel cell was dropped on the CNHs surface, the OCV increased. The voltage decreased in the low current range. This is called activation polarization, and it is a common phenomenon in fuel cells. To obtain further power, it is necessary to minimize activation polarization through methods such as employing another catalyst. [32, 33]

The CNHs' resistances were lower when the amounts of CNHs at 3 wt.% were increased, due to their 1D structural carbon properties. Besides, the developed fuel cell (CNHs, 3 wt.%) was also fabricated by the various amount of glucose concentrations (5, 10, 20 and 30) mM. When the glucose concentrations (5, 10, 20 and 30) mM were increased, the power density (2.9, 4.1, 6.5 and 8.64) μW/cm^2 also increased. So, the glucose concentration is an important issue for power generation. [34, 35] To conclude, the CMOS compatible glucose fuel cell with its anode side coated by 3 wt.% CNHs showed the highest performance. This corresponded with an OCV of 375 mV; the power was 0.41 μW, corresponding to a power density of 8.64 μW/cm^2. These values are promising for biomedical applications.

5.4. Summary

Here, a 17.5 mm × 0.7 mm solid-state CMOS-compatible glucose fuel cell was fabricated using CNHs in 30 mM glucose solution. The highest OCV (375 mV) was achieved at 3 wt.% of CNHs. The CMOS-compatible glucose fuel cell can deliver electric power to two connecting cells at room temperature. To conclude, this work exhibited different amounts of CNHs (1-7 wt.%) are performed on CMOS-compatible glucose fuel cells. This approach successfully enhanced the cell's OCV, and their electrical power could be applied to IoT technology into the healthcare industry.

References

1) K. Niitsu, S. Ota, K. Gamo, H. Kondo, M. Hori, and K. Nakazato, IEEE Trans. Biomed. Circuits Syst. 9, 607 (2015).
2) K. Niitsu, T. Kuno, M. Takihi, and K. Nakazato, IEICE Trans. Electron. E99-C, 663 (2016).
3) K. Niitsu, K. Yoshida, and K. Nakazato, Jpn. J. Appl. Phys. 55, 03DF13 (2016).
4) S. Zhu and G. Xu, Nanoscale 2, 2538-2549 (2010).
5) S. Iijima, M. Yudasaka, R. Yamada, S. Bandow, K. Suenaga, F. Kokai and K. Takahashi, Chem. Phys. Lett. 309, 165–170 (1999).
6) S. Arata, K Hayashi, Y Nishio, A. Kobayashi, K. Nakazato, and K. Niitsu, Jpn. J. Apply. Phys. 57, 04FM04 (2018).
7) S. Arata, K. Hayashi, X. Ge, S. Murakami, C. Dang Bui, A. Kobayashi, K. Niitsu, Jpn. J. Appl. Phys. 58, SBBG11 (2019).
8) K. Niitsu, T. Ando, A. Kobayshi, and K. Nakazato, Jpn. J. Appl. Phys. 56, 01AH04 (2017).
9) Jr. L.B. W., C. H. Shaw, and J. F. Castner, Enzyme Microb. Technol. 4 (3): P 6 (1982).

10) H. Sakai, T. Nakagawa, Y. Tokita, T. Hatazawa, T. Ikeda, S. Tsujimura, and K. Kano, Energy Environ. Sci. 2, 133–138 (2009).

11) A. Kobayashi, K. Ikeda, Y. Ogawa, H. Kai, M. Nishizawa, K. Nakazato, and K. Niitsu, IEEE Trans. Biomed. Circuits Syst. 11, 1313 (2017).

12) K. Niitsu, S. Ota, K. Gamo, H. Kondo, M. Hori, and K. Nakazato, IEEE Trans. Biomed. Circuits Syst. 9, 607 (2015).

13) K. Niitsu, T. Kuno, M. Takihi, and K. Nakazato, IEICE Trans. Electron. E99-C, 663 (2016).

14) K. Niitsu, K. Yoshida, and K. Nakazato, Jpn. J. Appl. Phys. 55, 03DF13 (2016).

15) Y.-T. Liao, H. Yao, A. Lingley, B. Parviz, and B. P. Otis, IEEE J. Solid State Circuits 47, 335 (2012).

16) F. Zhang and Y. Lian, IEEE Trans. Biomed. Circuits Syst. 3, 220 (2009).

17) M. Khayatzadeh, X. Zhang, J. Tan, W.-S. Liew, and Y. Lian, IEEE Trans. Biomed. Circuits Syst. 7, 583 (2013).

18) J. M. Song, J. Mobley, and T. Vo-Dinh, J. Chromatogr. B 783, 501 (2003).

19) T. Kuno, K. Niitsu, and K. Nakazato, Jpn. J. Appl. Phys. 53, 04EL01 (2014).

20) K. Niitsu, M. Sakurai, N. Harigai, T. J. Yamaguchi, and H. Kobayashi, IEEE J. Solid-State Circuits 47, 2701 (2012).

21) Y.-T. Liao, H. Yao, A. Lingley, B. Parviz, and B. P. Otis, IEEE J. Solid-State Circuits 47, 335 (2012).

22) X. Liu, L. Li, and A. J. Mason, IEEE Trans. Biomed. Circuits Syst. 8, 25 (2014).

23) R. Cabrera, I. Weaver, A. Banerjee, R. Sarpeshkar, and T. Thorsen, ECS Trans. 72, 31 (2016).

24) K. Niitsu, T. Ando, A. Kobayshi, and K. Nakazato, Jpn. J. Appl. Phys. 56, 01AH04 (2017).

25) J. Tan, W.-S. Liew, C.-H. Heng, and Y. Lian, IEEE Trans. Biomed. Circuits Syst. 8, 497 (2014).

26) B. I. Rapoport, J. T. Kedzierski, and R. Sarpeshkar, Plos one 7, e38436 (2012).

27) S. Kerzenmacher, M. Schroeder, R. Brämer, R. Zengerle, and F. von Stetten, J. Power Sources 195, 6516–6523 (2010).

28) K. Niitsu, T. Ando, A. Kobayshi, and K. Nakazato, Jpn. J. Appl. Phys. 56, 01AH04 (2017).

29) S. Kerzenmacher, J. Ducrée, R. Zengerle, and F. von Stetten, J. Power Sources 182, 1 (2008).

30) G. Wu, B. Q. Xu, J. Power Sources 174, 148–158 (2007).

31) M. A. Masadeh, K. Kuruvinashetti, M. Shahparni, P. Pillay, and M. Packirisamy, IEEE Trans. on Industrial Electronics 64, 1561 (2017).

32) S. Kerzenmacher, J. Ducrée, R. Zengerle, and F. von Stetten, J. Power Sources 182, 1 (2008).

33) S. Prilutsky, P. Schechner, E. Bubis, V. Makarov, E. Zussman and Y. Cohen, Electrochim. Acta 55, 3694–3702 (2010).

34) M. Z. Islam, S. Arata, K. Hayashi, A. Kobayashi, and K. Niitsu, Nanosci. Nanotechnol. Lett. 12, 642-645 (2020)

35) M. Z. Islam, S. Arata, K. Hayashi, A. Kobayashi and K. Niitsu, Sens. Mater. 32, 2597–2605 (2020)

Supplementary information

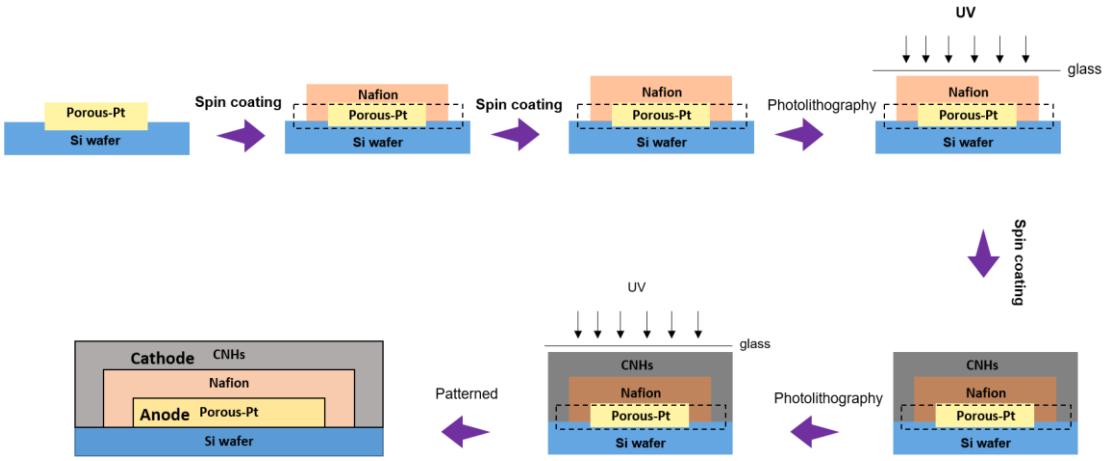

Fig. 5-S1 Systemic structure of the pattern using spin coating and photolithography process on Si wafer.

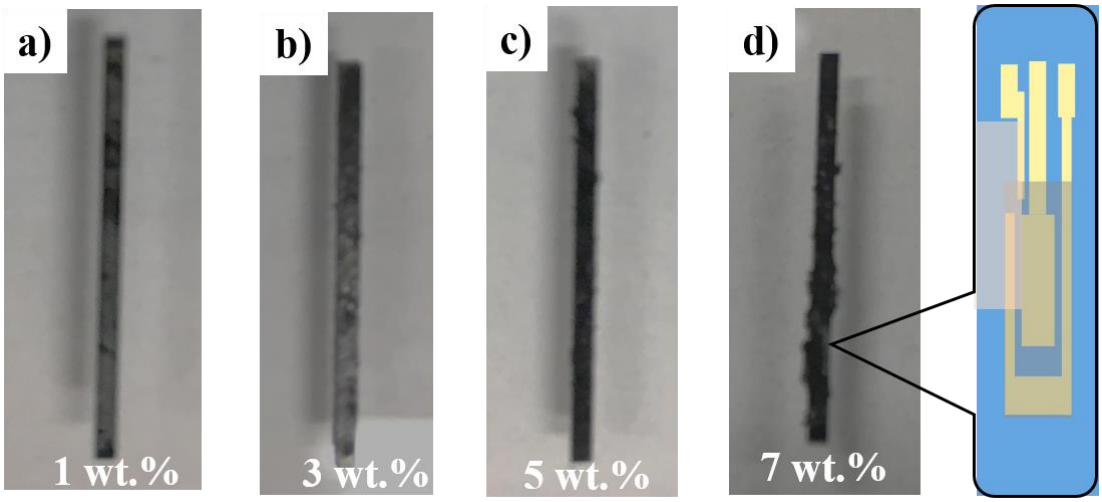

Fig. 5-S2 Photographs of the CMOS-compatible fuel cells fabricated with CNHs: a) 1 wt.%, b) 3 wt.%, c) 5 wt.%, and d) 7 wt.%.

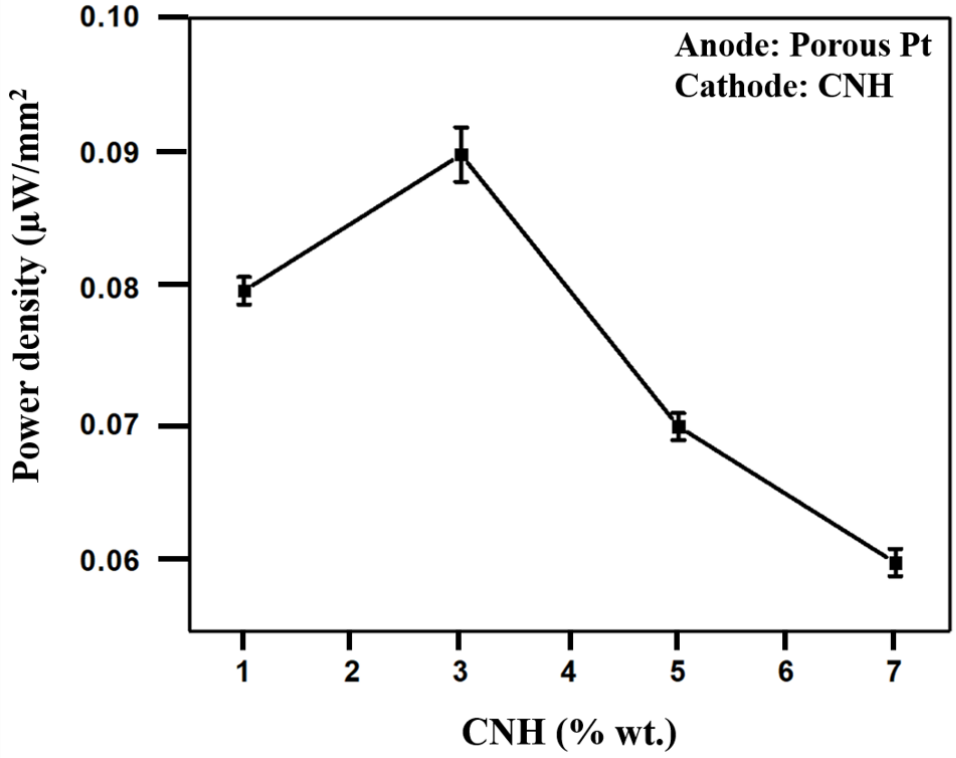

Fig. 5-S3 Power density obtained from the electrode surface area, compared with CNH wt.% (1, 3, 5, and 7 wt.% respectively).

Chapter 6

Summary

Chapter 6 – Summary

In the summary, we investigated palm oil is successfully converted to nanocarbons (W containing) by SPP and provided the high electrical conductivity and ORR activity in alkali and acid medium. The organic solvents are synthesized the nanocarbons (N, O and W containing) by SPP with high synthesis rate and catalytic activity site of ORR without thermal treatment and commercial Pt/C catalyst. The W containing nanocarbons of palm oils are showed high electrical conductivity, enhanced OOR activity and low synthesis rate compared with the organic solvents of N, O and W containing nanocarbons are provided the low electrical conductivity, higher electrochemical activity and higher synthesis rate without thermal treatment and the commercial Pt/C catalyst. And the finally, the solid state bio fuel cell fabricated by carbon nanohorns for biomedical applications.

The palm oils is cracking to nanocarbon by SPP requires the further studies for the synthesis rate and their applications. All experimental results and conclusions were discussed during Chapter 2−5.

Chapter 2 presents the enhancement of electrical conductivity and Oxidation Reduction Reaction (ORR) activity of tungsten carbide/carbon (WC/C) nanocomposite was successfully synthesized from palm oil by solution plasma process (SPP). The properties of the synthesized WC/C nanocomposite were varied by using a different frequency. The electrical conductivity increased with the frequencies. The highest electrical conductivity was 4.27×10^{-2} S cm^{-1}, which is higher than that of Ketjen Black (7.37×10^{-3} S cm^{-1}). The WC/C had a surface area of 160 m^2 g^{-1}, a pore volume of 0.53 cm^3 g^{-1}, an average pore diameter of 16.29 nm, a basal

plane crystallite size of 18.0 nm, and an average compound granule diameter of less than 100 nm. The cyclic voltammetry measurement was showed that the ORR activity of WC/C was obtained the good performance in alkaline solution for fuel cell application.

Chapter 3 focuses on nanocarbons synthesized by SP from the palm oils. The nanocarbons were covered enhanced electrical conductivity of nanocarbons, which is referred to the nanocarbons-encapsulated WC (tungsten carbides). In this study, we aimed to evaluate the structure and the properties of nanocarbons-encapsulated WC to provide the nanocarbons-encapsulated. The solution plasma was generated by the bipolar pulsed power supply through two tungsten electrodes using 2 μs pulse widths and frequencies (100, 150, and 180 kHz) for 30 min. Conversion percentage of the oil to WC- encapsulated nanocarbon (% yield) was increased with frequency. The obtained X-ray diffraction patterns are showed the crystalline structure. The electrochemical properties indicate that the ORR activity in an acidic medium under saturated O_2 significantly disappears in the case of the nanocarbon-encapsulated WC synthesised in the high frequency (180 kHz). The synthesized nanocarbons-encapsulated WC might be applied in data storage and energy applications.

Chapter 4 reveals that nanocarbons (N, O and W containing) were successfully synthesized from benzene (BZ), nitro-benzene (BZ-NO_2) and aniline (BZ-NH_2) by Solution Plasma Process (SPP). The synthesized nanocarbons were investigated. The highest synthesis rate of nanocarbon of BZ was 40 mg min^{-1}. The Transmission electron microscopy (TEM) morphology showed that the nanocarbons sizes were 15-25 nm. The cyclic voltammetry (CV) were exhibited in an acidic medium that oxygen reduction reaction (ORR) of nanocarbons. Nanocarbons of BZ-NH_2 have obtained a high special capacity of 15500 mAh/g carbon at the discharge rate of 0.1 mA/cm^2 with the 1.0 mg carbon loading for the lithium (Li)-air battery. An important reaction of ORR in Li-air battery and fuel cells for the applications of next-generation batteries and energy conversion devices.

Chapter 5 shows that this study details the development of a solid-state complementary metal-oxide semi- conductor (CMOS)-compatible bio fuel cell, consisting of various amounts (% wt.) carbon nanohorns (CNHs). It was fabricated on an anode area using one-dimensional (1D) structural CNHs, which express an open-circuit voltage (OCV) of 375 mV, the power density of 8.64 μW/cm2 and current density 23.05 μA/cm2 in 30 mM glucose solution. The cell can be manufactured via a CMOS fabrication process, using materials biocompatible with the human body. The CNHs enhanced the fuel cell due to their high electrocatalytic ability. The highest power is 0.42 μW. Power generation is the main challenge for developing bio fuel cells to make the implantable devices that can be used for biomedical applications.

In this thesis, solution plasma process is an excellent technic to synthesize the nanocarbons from the palm oils and the organic solvents. The W containing nanocarbons were successfully synthesized from palm oils by SPP with their high electrical conductivity, enhanced OOR activity and low synthesis rate compared with the organic solvents of N, O and W containing nanocarbons shows the low electrical conductivity, higher electrochemical activity and higher synthesis rate without thermal treatment and the commercial Pt/C catalyst. And the finally, the solid state bio fuel cell is fabricated by carbon nanohorns to make the implantable devices that can be used for biomedical applications.

Achievement

List of publication

[1] M. Z. Islam, A. Watthanaphanit, S. Chae, K. Niitsu and N. Saito, “High electrical conductivity and ORR activity of tungsten carbide/carbon nanocomposite synthesized from palm oil by solution plasma process”, Materials Express, 2020, (Accepted).

[2] M. Z. Islam, A. Watthanaphanit, S. Chae, K. Niitsu and N. Saito, “Structure and properties of nanocarbons-encapsulated WC synthesized by solution plasma process in palm oils”, Materials Express, 2020, (Accepted).

[3] M. Z. Islam, A. Watthanaphanit, S. Chae, and N. Saito, “Li-air battery and ORR catalytic of nanocarbon produced on synthesis rate by solution plasma process”, Materials Advances, 2021 (Accepted).

[4] M. Z. Islam, N. Matsuyama, G. Chen, A. Kobayashi, Y. Momoi and K. Niitsu, “A Needle-type complementary metal oxide semiconductor-compatible glucose fuel cell fabricated by carbon nanohorns for biomedical applications”, Electrochemistry (Tokyo), 88 (4), 333–335 (2020).

List of presentation in international conferences

[1] M. Z. Islam, M. A. Bratescu and N. Saito, “Nanocarbon materials synthesized by solution plasma process for their catalytic activity”, The 79th JSAP Autumn Meeting 2018, Nagoya Congress Center, Nagoya, Japan, 2018.

[2] M. Z. Islam, M. A. Bratescu and N. Saito, “Nanocarbon composites synthesized from vegetable oils by solution plasma process”, The Third Seminar on JSPS Core-to-Core Program (B. Asia-Africa Science Platforms) “Establishment of Research Hub for Compact Mobility

Model in the ASEAN Region", Nagoya University, Nagoya, Japan, 2018.

[3] M. Z. Islam, K. Hashimi, M. A. Bratescu and N. Saito, "The Structure and Properties of Nanocarbons-encapsulated WC Synthesized by Solution Plasma in Palm Oils", The 4th International Symposium on Hybrid Materials and Processings, HyMaP 2017, Guerinnarae Hotel, Haeundae, Busan, South Korea, 2017.

[4] M. Z. Islam, A. Watthanaphanit, and N. Saito, "Synthesis of palm to smart carbon materials by the solution plasma processing", The 9th Asia Pacific International Symposium on the Basics and Applications of Plasma Technology (APSPT-9)/ 28th symposium of on plasma Science and Materials (SPSM-28), Nagasaki University, Japan, 2015.

[5] M. Z. Islam, A. Watthanaphanit, and N. Saito, "Conversion of palm oil to carbon materials by plasma discharge in solution", The 10th Anniversary Asian-European International Conference on Plasma Surface Engineering (AEPSE2015), Ramada Plaza Jeju Hotel, Jeju, Republic of Korea, 2015.

[6] M. Z. Islam, A. Watthanaphanit, and N. Saito, "Carbon production from palm oil by plasma discharge in solution", The Mining and Materials processing Institute of Japan (MMIJ)-2015, Ehime University, Japan, 2015.

List of presentation in domestic conferences

[1] M. Z. Islam, A. Watthanaphanit, and N. Saito, "Synthesis of carbons from palm oil by solution plasma process and their characterizations", 4 inter-university cooperation young researchers Development Institute Materials science - to support the Next-Generation Green Technology, Nagano, Japan, 2015.

Acknowledgements

First of all, I would like to thank you very much to my supervisor Prof. Nagahiro SAITO (Department of Chemical Systems Engineering, Graduate School of Engineering, Nagoya University, Japan). He is an excellent researcher, supervisor and great human bring. He gave me an opportunity to do the research. During my study, I was received his always kind advices, support, encourage and the positive environment in Nagoya University, Japan.

To my thesis committee members, I would like to thank you very much to Prof. Ryoichi ICHINO (Graduate School of Engineering, Nagoya University, Japan), Prof. Motonobu GOTO (Graduate School of Engineering, Nagoya University, Japan), Associate Prof. Takeoka YUKIKAZU (Graduate School of Engineering, Nagoya University, Japan), I am really grateful for the suggestions for this thesis.

I would like to special thanks to Prof. Maria Antoaneta BRATESCU (Graduate School of Engineering, Nagoya University), Associate Prof. Kiichi NIITSU (Department of Electronics, Graduate School of Engineering, Nagoya University), Assistant Prof. Anyarat WATTHANAPHANIT (Department of Chemistry, Faculty of Science, Mahidol University, Thailand), Asst. Prof. Tomonaga UENO (Graduate School of Engineering, Nagoya University), and Assistant Prof. Sangwoo CHAE (Department of Chemical Systems Engineering, Graduate School of Engineering, Nagoya University) for kind help to this thesis.

I want to say thanks to all of the Prof. SAITO laboratory members, especially, Mrs. Eriko KONDO (Secretory), Mr. Akihito Yoshida (my tutor), Dr. Shimpei NEMOTO, Dr. Hyemin KIM, Dr. Tomohito SUDARE, Dr. Tetsunori MORISITA, Dr. Kyusung KIM, Dr. Akceoglu GARBIS, Dr. Hoonseung LEE and Dr. Wattanachai YAOWARAT for cooperation.

I want to say thanks to all members of Assoc. Prof. Kiichi NIITSU laboratory for their cooperation.

I want to say thanks to my uncles Assistant Professor Dr. Md. Nur ALAM (Lakehead University, Canada) and Mr. Md. Rabiul ALAM. They are always encouraged me to study and wishes the great success of my life.

I dedicate my thesis to my elder son Mr. Md Rafian ISLAM (2016.02.16), younger son Mr. Rafsan ISLAM (2018.12.04), my father Mr. Md. Shahidul ALAM, my mother MRS Rashida KHATUN and finally my wife MST. Laila SULTANA. They were sacrificed a lots.

I also want to dedicate my thesis to Prof. Nagahiro SAITO and Assoc. Prof. Kiichi NIITSU.

Finally, I would like to thanks to my all family members for their support.

Md. Zahidul ISLAM